

The Migrating Speed of Alternate Bars

Michihide Ishihara¹ and Hiroyasu Yasuda¹

¹Niigata University

November 22, 2022

Abstract

Alternate bars can spontaneously occur and develop in rivers. They are considered to be a wave phenomenon due to their geometrical features and propagation characteristics. Presently, there is insufficient knowledge about their propagation, which is an important wave phenomenon property. In this study, a flume experiment was conducted under the condition that alternate bars occur and develop. This investigation aims to understand the existence and the scale of migrating speed of these alternate bars. The bed and water levels during the occurrence and development of the alternate bars were measured frequently with a high spatial resolution. By comparing the geometrical changes in the bed shape, the migrating speed of the alternate bars has a spatial distribution that changes with time. To quantify the spatial distribution of the migrating speed of the alternate bars, a hyperbolic partial differential equation for the bed level and migrating speed formula were derived. A comparison of the measured values for the flume experiment showed that the derived formula is applicable. Using the formula of the migrating speed in this hyperbolic partial differential equation, the migrating speed was verified to have a spatial distribution. In addition, the distribution changes with the development of the alternate bars over time. This study demonstrates that the dominant physical quantity of the migrating speed is the energy slope from the experimental results and the migrating speed formula.

The Migrating Speed of Alternate Bars

Michihide Ishihara¹, Hiroyasu Yasuda²

¹Graduate School of Science and Technology, Niigata University, Niigata, Japan

²Research Institute for Natural Hazards & Disaster Recovery Niigata University, Niigata, Japan

Key Points:

- The spatial distribution of the migrating speed of alternate bars that occur in rivers was determined.
- A hyperbolic partial differential equation for the bed level and migrating speed formula were derived.
- The most dominant physical quantity of migrating speed of alternate bars is the energy slope.

Corresponding author: Hiroyasu Yasuda, hiro@gs.niigata-u.ac.jp

Abstract

Alternate bars can spontaneously occur and develop in rivers. They are considered to be a wave phenomenon due to their geometrical features and propagation characteristics. Presently, there is insufficient knowledge about their propagation, which is an important wave phenomenon property. In this study, a flume experiment was conducted under the condition that alternate bars occur and develop. This investigation aims to understand the existence and the scale of migrating speed of these alternate bars. The bed and water levels during the occurrence and development of the alternate bars were measured frequently with a high spatial resolution. By comparing the geometrical changes in the bed shape, the migrating speed of the alternate bars has a spatial distribution that changes with time. To quantify the spatial distribution of the migrating speed of the alternate bars, a hyperbolic partial differential equation for the bed level and migrating speed formula were derived. A comparison of the measured values for the flume experiment showed that the derived formula is applicable. Using the formula of the migrating speed in this hyperbolic partial differential equation, the migrating speed was verified to have a spatial distribution. In addition, the distribution changes with the development of the alternate bars over time. This study demonstrates that the dominant physical quantity of the migrating speed is the energy slope from the experimental results and the migrating speed formula.

1 Introduction

Periodic forms can spontaneously form along a river channel's bed surface. These forms are called riverbed waves because of their geometrical shapes and physical properties. Riverbed waves can be classified as small-scale, mesoscale, and large-scale based on spatial scales, which include the wavelength and wave height (Seminara, 2010). Small-scale riverbed waves have wavelengths on the scale of the water depth; meso-scale riverbed waves have wavelengths on the river width scale and wave heights on the water depth scale. Large-scale riverbed waves have larger scales. The target of this study is alternate bars that correspond to meso-scale riverbed waves. Alternate bars are riverbed waves that spontaneously form in rivers. They are located in sites from the alluvial fan to the natural embankment. When observing alternate bars from the sky with aerial photographs, the tip part is diagonally connected to the left and right riverbanks; a deep-water pool is located on the downstream side of this tip. In addition, it is known that the phase of the alternate bars propagates in the same way as the water surface waves during flooding.

Over the years, many studies have been conducted on alternate bars. One of the initial studies consisted of the flume experiments that were performed by Kinoshita (Ryosaku, 1961). Kinoshita conducted long-term flume experiment to understand the dynamics of the alternate bars that can produce meandering streams. According to this experiment experiments, he reported that 1) alternate bars have a globally uniform migrating speed and wavelength, 2) alternate bars in the early stages of development have short wavelengths and fast migrating speeds, and 3) the migrating speed becomes slower with the development of wavelengths. These results have been confirmed in subsequent studies (Ikeda, 1983; Fujita & Muramoto, 1985; Nobuhisa et al., 1999). In addition to the aforementioned conclusions, he proposed a formula to calculate the migration speed of the alternate bars based on the experimental results, with the Froude number and shear velocity as the dominant physical quantities. However, the validity of this formula has not been demonstrated in the same study.

Besides studies using flume experiments, several studies have applied mathematical analyses to understand the alternate bar phenomenon. Perhaps the first

63 mathematical study on alternate bars was that performed by Callander (Callander,
64 1969). He extended the stability analysis of Kennedy (Kennedy, 1963) for small-
65 scale bed waves to a two-dimensional plane problem and theoretically discussed the
66 physical quantities that govern the generation of meso-scale riverbed waves. This
67 study was the starting point for the research that aimed at predicting the conditions
68 under which alternate bars occur and the wavelength and wave height of the alter-
69 nate bars after development (Kuroki & Kishi, 1984; Colombini et al., 1987; Colombini
70 & Tubino, 1991; Tubino, 1991; Doelman et al., 1993). When considering the liter-
71 ature that used these stability analyses, the studies by Callander (Callander, 1969)
72 and Kuroki (Kuroki & Kishi, 1984) are important. They derived a formula to cal-
73 culate the migrating speed corresponding to the wave number that maximizes the
74 time amplification factor. The dominant physical quantities in the formula were
75 the Froude number, Shields number (shear velocity), bed slope, and wave number.
76 Moreover, in both the aforementioned studies, the value of the formula is compared
77 with the measured value. It has been reported that the reproducibility of the for-
78 mula to calculate the migrating speed is good.

79 With the rise of stability analysis, numerical analyses of the riverbed fluctua-
80 tions during the occurrence and development of alternate bars began to be carried
81 out. Shimizu et al. (Shimizu & Itakura, 1989) reported for the first time that nu-
82 merical analysis can satisfactorily reproduce each process of the occurrence and the
83 development of alternate bars. In recent years, Federici et al. (Federici & Seminara,
84 2003) reported the propagation direction of the riverbed waves by performing stabil-
85 ity and numerical analyses.

86 Recent studies that have used flume experiments (Lanzoni, 2000a, 2000b; Miwa
87 et al., 2007; Crosato et al., 2011, 2012; Venditti et al., 2012; Podolak & Wilcock,
88 2013) have investigated the effects of external factors such as the amount of sedi-
89 ment supply on the dynamics of the alternate bars. Crosato et al. (Crosato et al.,
90 2011, 2012) reported that alternate bars eventually shift from being migrating bars
91 to steady bars; they performed flume experiments and a numerical analysis to ver-
92 ify this. Next, Venditti et al. (Venditti et al., 2012) reported that when the sedi-
93 ment supply was interrupted after alternate bars occurred, the bed slope and shear
94 stress decreased, and the bars disappeared accordingly. Podolak et al. (Podolak &
95 Wilcock, 2013) also studied the response of alternate bars to sediment supply by in-
96 creasing the sediment supply during the occurrence and development of alternate
97 bars. It was demonstrated that a non-migrating bar changed to a migrating bar with
98 an increase in the bed slope and shear stress owing to increase in the sediment sup-
99 ply. In addition, Eekhout et al. (Eekhout et al., 2013) investigated the dynamics of
100 alternate bars in rivers for nearly three years and reported that the migrating speed
101 decreased as the wavelength and wave height of the alternate bars increased and the
102 bed slope decreased.

103 Thus far, the geometrical shape and physical properties of the alternate bars
104 have been investigated. Based on the previous studies, it is possible to predict the
105 presence or absence of the alternate bars and their geometric shapes to some extent.
106 However, there is very little understanding of the nature of the migration speed of
107 the alternate bars. Therefore, in this study, we focused on the migration speed while
108 focusing on the physics of alternate bars. As this is not well understood, we carried
109 out the following to clarify the existence and scale of the spatial distribution. Sec-
110 tion 2 describes the outline of the flume experiment that uses the Stream Tomog-
111 raphy (ST) method, which can simultaneously measure the geometric shapes of the
112 water surface and the bed surface with a high spatial resolution; the results are also
113 described. In Section 3, we assumed that the alternate bars can be regarded as a
114 wave phenomenon, and we derived a hyperbolic partial differential equation (HPDE)
115 for the bed level. In this study, the advection velocity that is given to the advection

116 term of the HPDE was used to calculate the migration speed of the alternate bars.
 117 In Section 4, the validity of the calculation formula that was derived in Section 3
 118 was verified based on the characteristics of the HPDE and the measured values of
 119 the bed level that was obtained in Section 2. In Section 5, the spatial distribution of
 120 the migration speed of the alternate bars is quantified using the formula to calculate
 121 the migration speed. Section 6 describes the results that were obtained in Section 5,
 122 and Section 7 summarizes the research results.

123 **2 Quantification of the Propagation Phenomenon in Alternate Bars** 124 **based on the Flume Experiment**

125 **2.1 Experimental Setup**

126 Figure 2 shows the plan view of the experiment flume. The experimental chan-
 127 nel consisted of a flume channel with a straight rectangular cross section. The flume
 128 had a length of 12.0 m, a width of 0.45 m, and a depth of 0.15 m. Fixed weirs with
 129 the same width as the flume were located 2.0 m from the upstream and downstream
 130 ends of the flume. Over the section between 2.0 m and 10.0 m from the upstream
 131 end that was sandwiched by these weirs, the initial bed of the channel for the exper-
 132 iment was a set flat bed. The bed was composed of a non-cohesive material with a
 133 mean diameter of 0.76 mm and had a thickness of 5.0 cm.

134 For the water supply to the channel, circulation-type pumping from a water
 135 tank at the downstream end to a water tank at the upstream end was adopted; the
 136 water was steadily supplied. The accuracy of the water discharge was confirmed us-
 137 ing an electromagnetic flowmeter.

138 **2.2 Experimental Condition**

139 The purpose of this study is to understand the existence and scale of the spa-
 140 tial distribution of the migration speed of the alternate bars. An alternate bar is a
 141 typical bed wave in a river that is attributed from an alluvial fan to a natural em-
 142 bankment.

143 Therefore, in the following experiments, we set the hydraulic conditions in
 144 which the alternate bars developed. It has been theoretically shown that the occur-
 145 rence of alternate bars can be estimated using the river width depth ratio. There-
 146 fore, in this study, we set BI_0^2/h_0 to 13.5, which corresponds to the occurrence area
 147 of the alternate bars in the area division map as shown by Kuroki and Kichi (Kuroki
 148 & Kishi, 1984). B is channel width, I_0 is the initial uniform bed slope, h_0 is the ini-
 149 tial uniform water depth. The bed slope of the flume is 1/160, the water discharge is
 150 1.5 L/s, the flow velocity and water depth are 0.28 m/s and 0.012 m, respectively, on
 151 the initial flat bed. The Shields number during the initial condition is 0.06, which is
 152 higher than the critical Shields number (0.034) that was obtained from Iwagaki's for-
 153 mula (Yuichi, 1956). The sediment supply along the upstream end was not provided.
 154 This is because by comparing the effect of the sediment supply with and without a
 155 preliminary experiment, it was observed that the spatial distribution of the migrat-
 156 ing speed of alternate bars and its temporal changes occurred without the sediment
 157 supply.

158 The water flow was carried out for 4 h during this experiment with the afore-
 159 mentioned conditions. At this time, alternate bars developed, and its propagation
 160 and shape change became slow.

2.3 Measurement Method for the Bed Surface and Water Surface

In this study, we used ST, which was developed by Hoshino et al., to measure the bed level and water level in a plane while the water is flowing. For details on the principles of the ST measurement, refer to Appendix A. In this study, the aforementioned measurements were performed with a spatial resolution of 2 cm² for every minute. The water depth was calculated from the difference between the water level and bed level. The water surface slope was calculated from the central spatial difference between the water levels.

2.4 Measurement Results

This section explains the propagation phenomenon of alternate bars using Fig. 3 and Fig. 4 based on the results of the high spatial resolution that was measured by ST.

Figure 3 shows the plan view of the deviation of the bed level by ST. The origin of the vertical coordinate of the ST is the flume bottom. Therefore, the water level and bed level represent the height from the bed of the flume. In this study, we measured the bed level at 1-minute intervals using ST. However, the results at 20-minute intervals indicate that a clear change can be easily confirmed under the set of hydraulic conditions that are shown. In this study, the initial bed surface was created so that it was as flat as possible. However, it was difficult to obtain a perfectly flat bed due to the accuracy limit of the bed surface that shapes the setup. It has been confirmed that the alternate bars, which occurred and developed under the aforementioned initial conditions, are almost the same as that developed in previous studies (Ryosaku, 1958; Federici & Seminara, 2003; Crosato et al., 2011; Venditti et al., 2012; Podolak & Wilcock, 2013).

First, the bed shape did not change from the flat bed as the initial condition (Fig. 3(a),(b)). Second, it was possible to see the bed topography in which the deposition and scouring are alternately repeated in the downstream direction, that is 1.0 m, 2.5 m, and 4.0 m from the upstream end; thus, it was possible to confirm that the alternate bars occurred (Fig. 3(c)). In this study, we defined 40 min, in which the geometric features of the alternate bars were confirmed from the measured result by the ST, as the occurrence time of the alternate bars. The alternate bars developed the topography over time; they were deposited more on the riffle side and scoured more on the pool. Subsequently, the entire alternate bars moved gradually in the downstream direction. The development and propagation of the alternate bars was significant from 40 min to 140 min (Fig. 3(c) to (h)). However, there was minimal development or propagation after 140 min (Fig. 3 (h) to (m)). From this result, comparing the migrating speed of the alternate bars during the early stage of development with the migrating speed of the fully developed alternate bars, it can be observed that the migrating speed in the former state is faster and the in latter is slower. Figure 4 shows the longitudinal distribution of the deviation in the bed level on the green dotted line in Fig. 3. Figure 4 shows (a) the initial stage of the experiment, (b) the occurrence of the alternate bars, (c) the intermediate stage of the experiment, and (d) the final stage of the experiment. Figure 4 shows three results, where each one is 20 min apart. First, the deviation of the bed level was confirmed to maintain a nearly flat bed from 1 min to 20 min (Fig. 4(a)). After (b) 40 min, two bed undulations developed that were 1.5 m and 4.0 m from the upstream end. The bed undulations developed their amplitudes and propagated in the downstream direction. As a result, ST was confirmed to observe the wave nature of the alternate bars.

The linear wave theory indicates that the phase propagates without deforming the waveform if a wave propagates with a spatial and temporal constant migrating

212 speed. Conversely, in the nonlinear wave theory, in which the migrating speed has a
 213 spatial distribution and temporal changes, the wave propagates with deformation of
 214 the waveform. From the viewpoint of the aforementioned wave theories, it is inferred
 215 that the migrating speed of the alternate bars at the time of the occurrence of the
 216 alternate bars in (b) has a spatial distribution; it changes with time and has nonlin-
 217 ear wave properties. Conversely, in (c) the intermediate stage of the experiment and
 218 (d) the final stage of the experiment, there was no deformation of the waveform and
 219 propagation. Thus, it was inferred that the migrating speed was almost zero; more-
 220 over, it is presumed that the wave nature was lost (Fig. 4(c),(d)).

221 **3 Derivation of the Calculation Formula for the Migrating Speed** 222 **of the Alternate Bars**

223 As shown in the previous section, the measurement results of this study show
 224 the wave nature in the process of the occurrence and development of the alternate
 225 bars. These findings are similar to what has been reported in the literature (Ryosaku,
 226 1958; Federici & Seminara, 2003; Crosato et al., 2011; Venditti et al., 2012; Podolak
 227 & Wilcock, 2013). In other words, there is scope for quantifying the spatial distribu-
 228 tion of the migration speed by an indirect method that uses a mathematical model
 229 such as the HPDE (Fujita et al., 1985), which is suitable for describing the wave phe-
 230 nomena. The formula for calculating the migration speed is also derived from the
 231 stability analysis (Callander, 1969; Kuroki & Kishi, 1984). However, because the for-
 232 mula calculates the migrating speed for each wave number, the spatial distribution
 233 of the migrating speed cannot be quantified. Therefore, in this study, we can use
 234 the HPDE for the bed level z and quantify the spatial distribution of the migration
 235 speed of the alternate bars using the advection velocity of the advection term that
 236 has the same formula.

237 This section describes the derivation process of the HPDE for the bed level
 238 z . In addition, four different formulas can be obtained depending on the physical as-
 239 sumptions. This includes whether the dimension is one-dimensional or two-dimensional,
 240 and whether the flow is stationary or unsteady. First, regarding the stationarity of
 241 the flow, as it was confirmed that the non-stationary state in the phenomenon tar-
 242 geted by this study is very small from the verification results that are described in
 243 Appendix B, we decided to deal only with the stationary state. In terms of the di-
 244 mensions, the geometric shape of the alternate bars and the flow there each has two-
 245 dimensional plane characteristics. Therefore, we decided to derive a two-dimensional
 246 stationary equation. The derivation of the HPDE for the bed level can be used for
 247 the continuous equation of the sediment, sediment functions, and the equation of the
 248 water surface profile. For the derivation, the Exner equation was used as the contin-
 249 uous equation of the sediment, and the Meyer–Peter and Müller (M.P.M) formula
 250 was used as the sediment function and the two-dimensional equation of the water
 251 surface profile. The application of the HPDE to the various sediment functions was
 252 examined using a method that is described in the next section. In this study, the
 253 M.P.M formula, which is simple and has good applicability, was adopted. Vectors for
 254 the longitudinal Eq. (2) and transverse Eq. (3) for the sediment flux are assumed
 255 to match the flows. Equation (6) was used to calculate the Shields number. Above
 256 all, we derived the steady two-dimensional equation of the water surface profile (Eq.
 257 (4), Eq. (5)) to derive the HPDE for the bed level. For the details on the derivation
 258 process of the steady two-dimensional equation for the water surface profile, please
 259 refer to Appendix C.

$$260 \quad \frac{\partial z}{\partial t} + \frac{1}{1 - \lambda} \left(\frac{\partial q_{Bx}}{\partial x} + \frac{\partial q_{By}}{\partial y} \right) = 0 \quad (1)$$

$$262 \quad q_{Bx} = 8(\tau_* - \tau_{*c})^{3/2} \sqrt{sgd^3} \frac{u}{V} \quad (2)$$

263

$$q_{By} = 8(\tau_* - \tau_{*c})^{3/2} \sqrt{sgd^3} \frac{v}{V} \quad (3)$$

264

265

$$\begin{aligned} \frac{\partial h}{\partial x} = & -\frac{\partial z}{\partial x} - I_{ex} - \frac{3}{10} \frac{u^2}{gI_{ex}} \frac{\partial I_{ex}}{\partial x} \\ & + \frac{1}{5} \frac{uv}{gI_{ey}} \frac{\partial I_{ey}}{\partial y} - \frac{1}{2} \frac{uv}{gI_{ex}} \frac{\partial I_{ex}}{\partial y} \end{aligned} \quad (4)$$

266

267

$$\begin{aligned} \frac{\partial h}{\partial y} = & -\frac{\partial z}{\partial y} - I_{ey} - \frac{3}{10} \frac{v^2}{gI_{ey}} \frac{\partial I_{ey}}{\partial y} \\ & - \frac{1}{2} \frac{uv}{gI_{ey}} \frac{\partial I_{ey}}{\partial x} + \frac{1}{5} \frac{uv}{gI_{ex}} \frac{\partial I_{ex}}{\partial x} \end{aligned} \quad (5)$$

268

269

270

$$\tau_* = \frac{hI_e}{sd} \quad (6)$$

271

272

273

274

275

276

277

278

279

where: z is the bed level, t is the time, λ is the porosity of the bed, q_{Bx} is the longitudinal sediment flux, x is the distance of the longitudinal direction, q_{By} is the transverse sediment flux, y is the distance of the transverse direction, τ_* is the composite Shields number, τ_{*c} is the critical Shields number, s is the specific gravity of the sediments in water, g is the gravity acceleration, d is the sediment size, u is the longitudinal flow velocity, V is the composite flow velocity, v is the transverse of the flow velocity, and h is the depth. In addition, $I_{bx} = -\partial z/\partial x$ is the longitudinal bed slope, I_{ex} is the longitudinal energy slope, $I_{by} = -\partial z/\partial y$ is the transverse bed slope, I_{ey} is the transverse energy slope, and n is the coefficient of roughness.

280

281

First, by applying the chain rule of differentiation to $\partial q_{Bx}/\partial x$ in Eq. (1), we obtain the following.

282

$$\begin{aligned} \frac{\partial q_{Bx}}{\partial x} = & \frac{\partial q_{Bx}}{\partial \tau_*} \left(\frac{\partial \tau_*}{\partial h} \frac{\partial h}{\partial x} + \frac{\partial \tau_*}{\partial I_e} \frac{\partial I_e}{\partial x} \right) \\ = & \frac{\partial q_{Bx}}{\partial \tau_*} \left(\frac{I_e}{sd} \frac{\partial h}{\partial x} + \frac{h}{sd} \frac{\partial I_e}{\partial x} \right) \\ = & \frac{\partial q_{Bx}}{\partial \tau_*} \frac{I_e}{sd} \left(\frac{\partial h}{\partial x} + \frac{h}{I_e} \frac{\partial I_e}{\partial x} \right) \end{aligned} \quad (7)$$

283

284

In addition, $\partial I_e/\partial x$ in Eq. (7) becomes the following due to the application of the chain rule to differentiate the Manning flow velocity Eq. (8).

285

$$V = \frac{1}{n} I_e^{1/2} h^{2/3} \quad (8)$$

286

287

$$\frac{\partial I_e}{\partial x} = \frac{\partial I_e}{\partial h} \frac{\partial h}{\partial x} + \frac{\partial I_e}{\partial V} \frac{\partial V}{\partial x} = -\frac{4}{3} \frac{I_e}{h} \frac{\partial h}{\partial x} + 2 \frac{I_e}{V} \frac{\partial V}{\partial x} \quad (9)$$

288

289

Substituting Eq. (9) in Eq. (7) and rearranging this, we can obtain the following equation.

290

$$\frac{\partial q_{Bx}}{\partial x} = \frac{\partial q_{Bx}}{\partial \tau_*} \frac{I_e}{sd} \left(-\frac{1}{3} \frac{\partial h}{\partial x} + 2 \frac{h}{V} \frac{\partial V}{\partial x} \right) \quad (10)$$

291

$\partial q_{Bx}/\partial \tau_*$ in the aforementioned equation is as follows.

292

$$\frac{\partial q_{Bx}}{\partial \tau_*} = 12(\tau_* - \tau_{*c})^{1/2} \sqrt{sgd^3} \left(\frac{u}{V} \right) \quad (11)$$

293

294

Equation (4) is used for $\partial h/\partial x$. Substituting Eq. (4) and Eq. (11) in Eq. (10), Eq. (10) is as follows.

295

$$\begin{aligned} \frac{\partial q_{Bx}}{\partial x} = & 4(\tau_* - \tau_{*c})^{1/2} \sqrt{sgd^3} \left(\frac{u}{V} \right) \frac{I_e}{sd} \left(\frac{\partial z}{\partial x} + I_{ex} \right. \\ & \left. + \frac{3}{10} \frac{u^2}{gI_{ex}} \frac{\partial I_{ex}}{\partial x} - \frac{1}{5} \frac{uv}{gI_{ey}} \frac{\partial I_{ey}}{\partial y} + \frac{1}{2} \frac{uv}{gI_{ex}} \frac{\partial I_{ex}}{\partial y} + 6 \frac{h}{V} \frac{\partial V}{\partial x} \right) \end{aligned} \quad (12)$$

296 In addition, $\partial q_{By}/\partial y$ is arranged in the same process as Eq. (12), and the following
 297 equation is derived.

$$\begin{aligned}
 \frac{\partial q_{By}}{\partial y} &= 4(\tau_* - \tau_{*c})^{1/2} \sqrt{sgd^3} \left(\frac{v}{V} \right) \frac{I_e}{sd} \left(\frac{\partial z}{\partial y} + I_{ey} \right) \\
 &+ \frac{3}{10} \frac{v^2}{gI_{ey}} \frac{\partial I_{ey}}{\partial y} - \frac{1}{5} \frac{uv}{gI_{ex}} \frac{\partial I_{ex}}{\partial x} + \frac{1}{2} \frac{uv}{gI_{ey}} \frac{\partial I_{ey}}{\partial x} + 6 \frac{h}{V} \frac{\partial V}{\partial y}
 \end{aligned} \tag{13}$$

299 By substituting Eq. (12) and Eq. (13) in Eq. (1), the following HPDE for the bed
 300 level z is derived.

$$\frac{\partial z}{\partial t} + M_x \frac{\partial z}{\partial x} + M_x I_{ex} + M_x F_x + M_y \frac{\partial z}{\partial y} + M_y I_{ey} + M_y F_y = 0 \tag{14}$$

302 In the aforementioned equation, M_x is the advection velocity of the longitudinal
 303 component of the bed level z . It is assumed to be closely related to the migration
 304 speed of the longitudinal component of the alternate bars, which is the subject of
 305 this study. M_y is the transverse migration speed of the alternate bars. M_x and M_y
 306 are not velocities of the sediments; they are supposed to be the propagation veloci-
 307 ties of the bed level z . M_x and M_y are as follows.

$$M_x = \frac{4(\tau_* - \tau_{*c})^{1/2} \sqrt{sgd^3} \left(\frac{u}{V} \right) I_e}{sd(1 - \lambda)} \tag{15}$$

$$M_y = \frac{4(\tau_* - \tau_{*c})^{1/2} \sqrt{sgd^3} \left(\frac{v}{V} \right) I_e}{sd(1 - \lambda)} \tag{16}$$

311 From Eq. (15) and Eq. (16), it can be observed that the dominant physical quanti-
 312 ties of the migrating speed are I_e and τ_* . In addition, F_x and F_y are as follows.

$$F_x = \frac{3}{10} \frac{u^2}{gI_{ex}} \frac{\partial I_{ex}}{\partial x} - \frac{1}{5} \frac{uv}{gI_{ey}} \frac{\partial I_{ey}}{\partial y} + \frac{1}{2} \frac{uv}{gI_{ex}} \frac{\partial I_{ex}}{\partial y} + 6 \frac{h}{V} \frac{\partial V}{\partial x} \tag{17}$$

$$F_y = \frac{3}{10} \frac{v^2}{gI_{ey}} \frac{\partial I_{ey}}{\partial y} - \frac{1}{5} \frac{uv}{gI_{ex}} \frac{\partial I_{ex}}{\partial x} + \frac{1}{2} \frac{uv}{gI_{ey}} \frac{\partial I_{ey}}{\partial x} + 6 \frac{h}{V} \frac{\partial V}{\partial y} \tag{18}$$

316 4 Verifying the Applications of the HPDE for the Bed Level z and 317 the Migrating Speed Formula based on the Measured Values

318 This section verifies the applicability of the HPDE for the bed level z and the
 319 formula for the migrating speed, which was described in the previous section. Verifi-
 320 cation is achieved using the values of the ST and hydraulic analysis.

321 4.1 Hydraulics required to verify applicability

322 This section describes the hydraulic quantities that are required to verify the
 323 applicability of the HPDE and the calculation formula for the migrating speed, as
 324 explained in the next section. As demonstrated from the HPDE and the calculation
 325 formula of the migrating speed shown in the previous section, the hydraulic quan-
 326 tities that are required for the verification of the applicability are the water depth,
 327 energy slope, and flow velocity. The water depth can be obtained from the bed level
 328 and water level that is measured by the ST. However, the flow velocity and energy
 329 slope that are paired with the water depth have not been measured; this measure-
 330 ment is generally difficult. Therefore, we determined the flow velocity and energy
 331 slope by performing a numerical analysis.

332 For the numerical analysis, Nays2D included in iRIC (<http://www.i-ric.org>)
 333 can solve the two-dimensional plane hydraulic analysis. It was conducted with a bed
 334 level that was measured by the ST as a fixed bed.

335 The arrangement interval of the calculation points was 2 cm, which is the same
 336 as the resolution of the ST in the transverse and longitudinal directions. The up-
 337 stream end boundary condition had a flow rate of 1.5 L /s; the downstream end
 338 boundary condition provided the measured water depth. In addition, the roughness
 339 coefficient was adjusted each time so that the calculated and measured values of the
 340 water depth matched and they were uniform over the entire section. Figure 5 shows
 341 the measured water depth. Figure 6 shows the difference between the measured wa-
 342 ter depth and the calculated value, which is dimensionless Δh_* . In addition, Fig.
 343 7 illustrates the calculated flow velocity. Of these, Δh_* represents the calculation
 344 accuracy of the numerical analysis. By focusing on Δh_* in Fig. 6, Δh_* is approxi-
 345 mately 10% for the entire channel at any time, regardless of the developmental state
 346 of the alternate bars. In all the areas where Δh_* is 60% or more, the water depth is
 347 very shallow. Most of these regions are not included when calculating the migrating
 348 speed. This is demonstrated from the plan view of the migrating speed in Fig. 10
 349 that is shown in the next section. Therefore, we decided to use the calculated value
 350 of this part as well. In the next section, we verify the applicability of the derived
 351 calculation formulas using these hydraulic quantities.

352 4.2 Verifying the Application of the Time Waveform for the Bed 353 Level and the Riverbed Fluctuation Amount

354 We verified the applicability of the calculation formula that is derived in the
 355 previous section from two points of view. First, can the time waveform of the mea-
 356 sured bed level be reproduced? Second, can the riverbed fluctuation amount that is
 357 measured in the entire section be reproduced? The verification results are described
 358 in this section.

359 4.2.1 Bed-level Time Waveform

360 The verification method that uses the time waveform at the bed level is de-
 361 scribed here. The HPDE from Eq. (14) that was derived in the previous section is
 362 numerically calculated as follows, and the amount of the riverbed fluctuation is be-
 363 tween Δz .

$$364 \Delta z = \left(-M_x \frac{\partial z}{\partial x} - M_x I_{ex} - M_x F_x - M_y \frac{\partial z}{\partial y} - M_y I_{ey} - M_y F_y \right) \Delta t \quad (19)$$

365 This calculation used the bed level and water depth that is measured with ST, as
 366 well as the calculated values of the energy slope and flow velocity based on the hy-
 367 draulic analysis that was described in the previous section. A time waveform at the
 368 bed level was obtained by repeating this numerical integration during each ST mea-
 369 surement time.

370 The applicability of the HPDE that was obtained in the previous section was
 371 investigated by comparing the time waveform of the bed level. This was calculated
 372 using the aforementioned method with the time waveform of the bed level that was
 373 observed by the ST. In this study, because the ST measurements were performed at
 374 1-min intervals, Δt in the aforementioned calculation was set to 1 min.

375 Figure 8 shows the time waveform at the bed level. Figure 8 shows the time
 376 waveforms of (a) the left bank side, (b) central part, and (c) right bank side at 6.0
 377 m from the upstream end; the red line shows the bed level of the measured value. In
 378 the figure, the blue line shows the bed level that is calculated from the calculation
 379 formula. By focusing on the measured values that are shown by the red line in Fig.
 380 8, (a) the bed level decreases on the left bank side, and (b) the bed level increases
 381 on the central part and (c) right bank side from the start of the water flow to 50
 382 min. In addition, it can be observed that the bed level of (a) and (b) settled down

and the bed level of (c) increased from 50 to 150 min for the water flow. After 150 min, the bed level increased slightly for (a), (b), and (c).

Next, by looking at the time waveform of the bed level with the calculation formula, the time waveform of the bed level is well reproduced from the start of the water flow to 100–120 min in Figures (a), (b), and (c). It can be confirmed that after 100 min, the reproducibility decreases on (a) the left bank side; after 150 min, the reproducibility decreases on (b) the center and (c) the right bank side. By overlooking the process from the occurrence to the development of alternate bars using Fig. 4 and Fig. 8, it was confirmed that the reproducibility of the time waveform, when the propagation of the alternate bars is remarkable, is good. Conversely, it was determined that the reproducibility becomes poor, especially in the sedimentary part when the propagation of the alternate bars is slow.

As mentioned earlier, the time waveform was obtained by setting the time integration interval to 1 min. Although this time interval cannot be simply compared, it is much larger than the time interval in a general numerical analysis. From this result, it was determined that the verification method that uses the aforementioned numerical integration and the applicability of the calculation formula that was derived in the previous section are excellent.

4.2.2 Riverbed Variation Amount

The verification in the previous section showed that the HPDE for Eq. (14) has sufficient applicability, but its applicability decreases as the alternate bars develop. In this section, we discuss how much of this reduced applicability occupies the entire waterway and where it occurs. This is achieved using the riverbed variation amount. The verification of the riverbed variation was performed using the following equation.

$$\Delta z_* = |\Delta z_{obs} - \Delta z_{cal}|/d \times 100 \quad (20)$$

where Δz_{obs} is the riverbed variation that was obtained from the bed level between the two times that were measured by the ST. In addition, Δz_{cal} is the amount of the riverbed variation by the HPDE and the calculation formula of the migration speed. Δz_* in the aforementioned equation is a dimensionless quantity that is obtained by dividing the difference between the measured value of the riverbed variation amount and the calculated value using the equation based on the particle size. In addition, the difference between the two shows how much the divergence is based on the particle size.

Figure 9 shows the plan view for the calculation accuracy of the riverbed variation Δz_* . Figure 9 shows the bed level, Δz_* from the top. In addition, (a) to (i) indicates the time zone in which the change is remarkable from the occurrence to the development at 10-min intervals. In addition, (i) to (l) indicates the time zone in which the change is slow until the end of the water flow at 40-min intervals. (a) Looking at the results for 1 min of water flow, Δz_* is generally within 100%, and the estimation accuracy of the waveform after 1 min at this time is the same as the particle size.

From (a) 1 min of water flow to (h) 70 min, it can be observed that Δz_* is generally within 100% of the entire channel. However, it can be observed that Δz_* increases at the front edge of the bar after 80 min of water flow in comparison to the other areas. From this, it is inferred that the applicability of this formula decreases at the front edge of the alternate bars where the water depth becomes shallow. Presently, the factors that reduce the applicability of the calculation formula have not been sufficiently identified; however, it is suggested that careful handling is required in places where the water depth becomes shallow. Conversely, it is unlikely

433 that alternate bars with a high wave height such that the water depth becomes ex-
 434 tremely shallow as considered in this experiment actually exists in an actual river;
 435 therefore, it is considered that the decrease in applicability at the aforementioned
 436 points is acceptable. It should be noted that there is a striped area where Δz_* is
 437 close to 500% on the side wall of the figure. This area is considered to occur owing
 438 to a decrease in the ST measurement accuracy. In addition, (b) an increase in Δz_*
 439 at the upstream end for 10 min of water flow is considered to occur owing to the
 440 same aforementioned reason. Therefore, in the following discussion, the striped pat-
 441 tern of Δz_* on the right bank side and Δz_* at the upstream end were excluded from
 442 consideration.

443 5 Quantification of the Migrating Speed for the Alternate Bars

444 The previous section confirmed that HPDE and the calculation formula for the
 445 migrating speed can reproduce the propagation phenomenon of the alternate bars.
 446 In this section, the migration speed of the alternate bars in each process during the
 447 occurrence and development is quantified using the calculation formula of the mi-
 448 grating speed.

449 5.1 Spatial Distribution of the Migrating Speed of the Alternate 450 Bars

451 Figure 10 shows a plan view of the dimensionless migrating speed that is ob-
 452 tained by dividing the migrating speed that is obtained from the calculation formula
 453 for the bed level by the initial uniform flow velocity. The dimensionless migrating
 454 speed was used to understand the magnitude of the running water velocity and bed
 455 velocity. In a stability analysis(Callander, 1969; Kuroki & Kishi, 1984) that was con-
 456 ducted in the past, by applying the dimensionless governing equation, the migrating
 457 speed that was made dimensionless during the uniform velocity flow is often used.

458 The figure shows the bed level and M/u_0 from the top. M is the magnitude
 459 migrating speed, u_0 is the uniform flow velocity. The area surrounded by the hatch
 460 in the figure is the area in which the Shields number does not exceed the critical
 461 Shields number (hereinafter referred to as the effective Shields number); in this area,
 462 the migrating speed is 0. It is demonstrated that (a) to (i) indicates the time zone in
 463 which the change is significant from the occurrence to the development of the alter-
 464 nate bars at 10-min intervals. In addition, (i) to (l) indicates the time zone in which
 465 the change is slow until the end of the water flow at 40-min intervals. It should be
 466 noted that the colors of the case law regarding the bed level and M/u_0 are different
 467 between (a) to (h) and (i) to (l).

468 First, by focusing on (a) 1 min of water flow in the figure, M/u_0 has almost no
 469 spatial distribution on a floor with an almost flat bed. It is also confirmed that the
 470 bed surface propagates uniformly at a speed of approximately 0.002. After the bed
 471 changes slightly from (b) 10 min to (c) 20 min, M/u_0 begins to have a spatial dis-
 472 tribution. Subsequently, the spatial distribution of M/u_0 changes significantly from
 473 (d) 30 min of water flow to (e) 40 min when the alternate bars occurred. Looking at
 474 this change with a spatial distribution from place to place, it can be observed that
 475 M/u_0 increases at the sedimentary part and the front edge of the alternate bars, and
 476 it decreases at other places. Subsequently, the spatial distribution of M/u_0 became
 477 clearer from (f) 50 min to (i) 80 min. In addition, before this time, it can be demon-
 478 strated that the area, where migrating speed is zero, is expanded on the downstream
 479 side of the front edge. In addition, (i) M/u_0 at 80 min of water flow decreased to
 480 approximately 0.001 or less, while excluding the sedimentary part. (l) The spatial
 481 distribution of the migrating speed at 240 min of the final time is not significantly
 482 different from the distribution of (i) 80 min, but the area, where migrating speed

483 is zero, is further expanded. In addition, M/u_0 also decreases slightly in the entire
484 channel.

485 Next, Fig. 11 illustrates a histogram that quantitatively shows the spatial dis-
486 tribution degree of M/u_0 at each time. The red and blue vertical lines in the fig-
487 ure represent the mean and mean \pm standard deviation of M/u_0 at each time, and
488 each value is shown at the top of the figure. First, (a) the shape of the histogram
489 after 1 min of water flow was concentrated around the average value of 0.157. In ad-
490 dition, because the standard deviation is 0.029, which is small with respect to the
491 mean value, it can be observed that the spatial distribution of M/u_0 at this time is
492 small. Then, from (b) 10 min of water flow to (e) 40 min of water flow when the al-
493 ternate bars occurred, the shape of the histogram became flat, and the mean value
494 of M/u_0 was 0.147, and the standard deviation was 0.051. Comparing (a) 1 min and
495 (e) 40 min of water flow, although the mean value decreased by approximately 4 %,
496 the standard deviation increased to nearly 40 % of the mean value. From this, it is
497 demonstrated that the spatial distribution of the migrating speed greatly expanded
498 from the flat bed to the occurrence of the alternate bars. After that, from (e) 40
499 min to (i) 80 min of water flow, the flattening of the histogram, the increase in the
500 standard deviation, and the decrease in the mean value of M/u_0 became more sig-
501 nificant. From this, the increase in the standard deviation is particularly significant,
502 and the standard deviation value during 80 min of water flow reaches 70 % of the
503 average value of M/u_0 . (i) After 80 min of water flow, there is no significant change
504 from (e) to (i). However, the average value of M/u_0 gradually increases over 240
505 min of the final time, and it decreases and the standard deviation increases. Com-
506 paring (a) 1 min of water flow and (k) 240 min, which was the final time, the mean
507 value of M/u_0 is 0.72 times, and the standard deviation is 4.8 times.

508 From these results, it was demonstrated that the migration speed of the alter-
509 nate bars has a spatial distribution, and this spatial distribution expands from the
510 stage of occurrence to the development of the alternate bars.

511 5.2 Scale of the Migrating Speed of the Alternate Bars

512 This section discusses the scale of the migration speed of the alternate bars. As
513 shown in the previous section, from Fig. 11, it can be confirmed that the migrating
514 speed has a spatial distribution and it gradually expands from 1 min of water flow
515 to 240 min, which was the final time. The non-dimensional migrating speed in the
516 figure is divided by the uniform flow velocity (0.28 m/s) on the flat floor. However,
517 the scale of the migrating speed is on the order of 10^{-4} to 10^{-3} of the uniform flow
518 velocity at any place, regardless of the developmental state of the alternate bars.
519 Therefore, it is inferred that the deformation rate of the bed surface is sufficiently
520 smaller than the deformation rate of the running water. This tendency is similar
521 to the result of the non-dimensional migrating speed that corresponds to the wave
522 number of the maximum development rate as described by Callander(Callander,
523 1969).

524 6 Discussion

525 In the previous sections, it was clarified that the migration speed of the alter-
526 nate bars has a spatial distribution, and this spatial distribution changes with time.
527 This section discusses the following three aspects of the migration speed of the alter-
528 nate bars.

6.1 Approximate Description of the most Dominant Physical Quantity of the Migrating Speed

This study derived a formula to calculate the migration speed and its applicability is confirmed. Therefore, by considering the mathematical structure of the same formula, it is possible to determine the most dominant physical quantity that controls the migration speed. As demonstrated in Eq. (15) and Eq. (16), the dominant physical quantities of the migrating speed are the Shields number and energy slope, which excludes the component decomposition of the migrating speed. Because the dominant physical quantities of the Shields number consist of the water depth and energy slope, it can be concluded that the dominant physical quantities of the migrating speed are the water depth and energy slope. In addition, the migrating speed is calculated by multiplying the depth and the energy slope as shown in Eq. (15) and Eq. (16). The depth in a river with alternate bars is generally on the order of 10^0 , and the energy slope in the rivers with alternate bars is on the order of 10^{-2} to 10^{-4} . Therefore, because the migration speed is the product of the water depth and energy slope, it is inferred that the energy slope is dominant in terms of regulating the magnitude of the migrating speed.

Figure 12 shows the relationship between the depth, energy slope, and migrating speed at each time. As demonstrated in Fig. 12, the relationship between the energy slope and migrating speed is nearly linear. Regarding the relationship between the depth and migrating speed, the migrating speed decreased with an increasing depth. From these results, it can be demonstrated that the migrating speed of the alternate bars is defined according to the energy slope.

It was previously demonstrated that the dominant physical quantity of the migrating speed is the energy slope. It is believed that an approximate description of the migrating speed is possible using the energy slope and a water surface slope, which is very similar to the energy slope. We verified whether the above approximate description is possible from Fig. 13. The red points show the relationship between M/u_0 and $0.4 \times I_e$, and the green point shows M/u_0 and $0.4 \times I_w$ in Fig. 13. I_w is the value that is obtained by the central spatial difference of the water level that is measured by the ST. Each correlation coefficient is shown on the upper side of Fig. 13. Furthermore, 0.4, which is multiplied by I_e and I_w , is a coefficient that is determined by the particle size. This is one of the variables on the denominator side of Eq. (15) and Eq. (16).

First, it can be observed that the relationship between M/u_0 and $0.4 \times I_e$ is a nearly one-to-one relationship at all times. Furthermore, both relationships have a highly positive correlation because the correlation coefficients are over 0.99, on average. Second, it can be demonstrated that there is some variation in the relationship between M/u_0 and $0.4 \times I_w$, but it is also a nearly one-to-one relationship at all times. Furthermore, both relationships have a highly positive correlation because the correlation coefficients are over 0.96 on average.

From these results, it was determined that the dominant physical quantity of the alternate bars is the energy slope, and the migration speed can be approximated using the energy slope and water surface slope.

6.2 Comparison of the Migrating Speed and the Stability Analysis

The migration speed based on the stability analysis (Callander, 1969; Kuroki & Kishi, 1984) has four dominant physical quantities: the Froude number, Shields number, bed slope, and wavenumber. In addition, the migration speed that was obtained from the HPDE, which was discussed in the previous section, is dominated by the Shields number and energy slope. The migration speed that was obtained from

each stability analysis and the HPDE both have the water depth and energy slope as the dominant physical quantities. However, the migration speed that was obtained from the stability analysis was limited to those that correspond to any wavenumber.

6.3 Decreasing Factor for the Migrating Speed of the Alternate Bars

This subsection discusses the decreasing factor for the migrating speed of the alternate bars. Figure 14 shows the average longitudinal distributions of the migrating speed, energy line, hydraulic grade line, and bed line over time. The sediment condition for the flume experiment in this study is that there is no sediment supply. Therefore, this study confirmed that the bed level decreases with the passage of time along the upstream side of the movable bed. At the final time, the bed level decreased significantly from the upstream end to a point that is 3.5 m away. It can be demonstrated that (b) the water level and energy head in this section have decreased compared to the initial stage, and the riverbed slope and energy slope become more gentle. In addition, (a) the migrating speed, which was calculated from Eq. (15) at the final time in this section, is lower than that during the beginning of the water flow.

A previous study by Eekhout et al. (Eekhout et al., 2013), which observed the occurrence and development process of the alternate bars in rivers, reported that the bed slope decreased while reducing the migration speed of the alternate bars. The results shown in Fig. 14 are consistent with those reported by Eekhout et al.

As mentioned earlier, the dominant physical quantity of the migrating speed of the alternate bars is the energy slope. The decrease in the migrating speed, which was confirmed by the flume experiments in this study and the observations in the actual river by Eekhout et al., should be interpreted as a decrease in the migration speed of the alternate bars due to the decrease in the riverbed slope rather than the decrease in the migrating speed with the development of the alternate bars.

7 Conclusion

In this study, we first conducted a flume experiment under the condition that alternate bars can occur and develop. We measured the hydraulic quantity and bed shape with a high spatial resolution. Next, we quantified the migrating speed of the alternate bars using the measured values that were obtained in the flume experiment and the calculation formula. This study determined that the migration speed of the alternate bars has a spatial distribution and it changes with time. The results of this study are presented below.

- 1) We were able to measure the water level and bed level with a high resolution while continuing the water flow. In addition, the water level and bed level of the occurrence and development process of the alternate bars are measured, and it is demonstrated that the migrating speed of the alternate bars has a spatial distribution from the measured geometric shape of the bed surface.
- 2) The HPDE for the bed level z and the formula of the migrating speed were derived to quantitatively determine the migrating speed of the alternate bars. By comparing the measured values of the flume experiment, it was demonstrated that the formula can appropriately describe the propagation phenomenon of the alternate bars.
- 3) By calculating the migrating speed of the alternate bars based on the aforementioned formula, it was clarified that the migrating speed of the alternate bars has a spatial distribution. In addition, the spatial distribution changes with the development of the bars over time, which was unconfirmed in the literature.

- 628 4) The dominant physical quantity of the migrating speed is the energy slope
 629 based on the results of the experiment and calculation formula. In addition,
 630 by comparing the scales of I_e and I_w with the non-dimensional migrating
 631 speed, it is suggested that the non-dimensional migrating speed can be de-
 632 scribed using I_e and I_w ; the behavior of the bars in the rivers can also be ex-
 633 plained by I_e and I_w .
- 634 5) It was observed that the migrating speed of the alternate bars is about three
 635 to four orders of magnitude smaller than the initial uniform flow velocity, re-
 636 gardless of the developmental state and the location of the bars.

637 It was found that the decrease in the applicability of the HPDE for the bed
 638 level and calculation formula of migration speed for the alternate bars, which was
 639 derived in this study, occurs in the sediment parts with extremely shallow water
 640 depth. Therefore, it is difficult to apply the aforementioned formula. However, it is
 641 unlikely that alternate bars, which has sediment parts with extremely shallow water
 642 depth, will occur in actual rivers, so this problem is not considered to be a practical
 643 problem.

644 Previous studies have revealed that the bank failure and the channel evolution
 645 are closely related to alternate bars (Ryosaku, 1957; Callander, 1969). In the future,
 646 we will quantify the spatial distribution of the migration speed of alternate bars in
 647 actual rivers, and consider the above relationship.

648 Acknowledgments

649 The data used in this study can be accessed at <https://doi.org/10.4121/14384999>.
 650 For details of the data, please refer to the enclosed README.md. We would like to
 651 thank Editage (www.editage.com) for English language editing.

652 References

- 653 Callander, R. A. (1969). Instability and river channels. *Journal of Fluid Mechanics*,
 654 *36*(3), 465-480. doi: 10.1017/S0022112069001765
- 655 Colombini, M., Seminara, G., & Tubino, M. (1987). Finite-amplitude alternate bars.
 656 *Journal of Fluid Mechanics*, *181*, 213-232. doi: 10.1017/S0022112087002064
- 657 Colombini, M., & Tubino, M. (1991). Finite-amplitude free bars: A fully nonlinear
 658 spectral solution. in *Sand Transport in Rivers, Estuaries and the Sea*, edited by
 659 R. Soulsby and R. Bettes, A. A. Balkema, Brookfield, Vt., 163-169.
- 660 Crosato, A., Desta, F. B., Cornelisse, J., Schuurman, F., & Uijttewaal, W. S. J.
 661 (2012). Experimental and numerical findings on the long-term evolution of mi-
 662 grating alternate bars in alluvial channels. *Water Resources Research*, *48*(6).
 663 doi: 10.1029/2011WR011320
- 664 Crosato, A., Mosselman, E., Beidmariam Desta, F., & Uijttewaal, W. S. J. (2011).
 665 Experimental and numerical evidence for intrinsic nonmigrating bars in allu-
 666 vial channels. *Water Resources Research*, *47*(3). doi: 10.1029/2010WR009714
- 667 Doelman, A., de Swart, H., & Schielen, R. (1993, 07). On the non-linear dynamics of
 668 free bars in straight channel. *Journal of Fluid Mechanics*, *252*, 325 - 356. doi:
 669 10.1017/S0022112093003787
- 670 Eekhout, J. P. C., Hoitink, A. J. F., & Mosselman, E. (2013). Field experiment
 671 on alternate bar development in a straight sand-bed stream. *Water Resources*
 672 *Research*, *49*(12), 8357-8369. doi: 10.1002/2013WR014259
- 673 Federici, B., & Seminara, G. (2003). On the convective nature of bar instability.
 674 *Journal of Fluid Mechanics*, *487*, 125-145. doi: 10.1017/S0022112003004737
- 675 Fujita, Y., Koike, T., Furukawa, R., & Y., M. (1985). Experiments on the initial
 676 stage of alternate bar formation. *Disaster Prevention Research Institute Annu-
 677 als (in Japanese)*, *28*(B-2), 379-398.

- 678 Fujita, Y., & Muramoto, Y. (1985). Studies on the process of development of al-
679 ternate bars. *Bulletin of the Disaster Prevention Research Institute*, 30(3),
680 55-86.
- 681 Ikeda, H. (1983). Experiments on bedload transport, bed forms, and sedimentary
682 structures using fine gravel in the 4-meter-wide flume..
- 683 Kennedy, J. F. (1963). The mechanics of dunes and antidunes in erodible-
684 bed channels. *Journal of Fluid Mechanics*, 16(4), 521-544. doi: 10.1017/
685 S0022112063000975
- 686 Kuroki, M., & Kishi, T. (1984). Regime criteria on bars and braids in allu-
687 vial straight channels. *Proceedings of the Japan Society of Civil Engineers*,
688 1984(342), 87-96. doi: 10.2208/jscej1969.1984.342_87
- 689 Lanzoni, S. (2000a). Experiments on bar formation in a straight flume: 1. uni-
690 form sediment. *Water Resources Research*, 36(11), 3337-3349. doi: 10.1029/
691 2000WR900160
- 692 Lanzoni, S. (2000b). Experiments on bar formation in a straight flume: 2. graded
693 sediment. *Water Resources Research*, 36(11), 3351-3363. doi: 10.1029/
694 2000WR900161
- 695 Miwa, H., Daisdo, A., & Katayama, T. (2007). Effects of water and sediment dis-
696 charge conditions on variation in alternate bar morphology. *Proceedings of hy-*
697 *draulic engineering (in japanese)*, 51, 1051-1056. doi: 10.2208/prohe.51.1051
- 698 Nobuhisa, N., Yoshio, M., Yoshihiko, U., Takashi, H., Masayuki, Y., Yasuhiko, T., &
699 Michiaki, I. (1999). On the behaviour of alternate bars under several kinds of
700 channel conditions. *PROCEEDINGS OF HYDRAULIC ENGINEERING (in*
701 *japanese)*, 43, 743-748. doi: https://doi.org/10.2208/prohe.43.743
- 702 Podolak, C. J. P., & Wilcock, P. R. (2013). Experimental study of the response of
703 a gravel streambed to increased sediment supply. *Earth Surface Processes and*
704 *Landforms*, 38(14), 1748-1764. doi: 10.1002/esp.3468
- 705 Ryosaku, K. (1957). Formation of "dunes" on river-bed. *Transactions of the*
706 *Japan Society of Civil Engineers in Japan(in Japanese)*, 1957(42), 1-21. doi:
707 10.2208/jscej1949.1957.1
- 708 Ryosaku, K. (1958). Experiment on dune length in straight channel. *Journal of*
709 *the Japan Society of Erosion Control Engineering (in japanese)*, 1958(30), 1-8.
710 doi: 10.11475/sabo1948.1958.30_1
- 711 Ryosaku, K. (1961). Investigation of channel deformation in ishikari river. *Rep.*
712 *Bureau of Resources, Dept. Science & Technology, Japan. (in japanese)*.
- 713 Seminara, G. (2010). Fluvial sedimentary patterns. *Annual Review of Fluid Mechan-*
714 *ics*, 42(1), 43-66. doi: 10.1146/annurev-fluid-121108-145612
- 715 Shimizu, Y., & Itakura, T. (1989). Calculation of bed variation in alluvial channels.
716 *Journal of Hydraulic Engineering*, 115(3), 367-384. doi: 10.1061/(ASCE)0733
717 -9429(1989)115:3(367)
- 718 Tubino, M. (1991). Growth of alternate bars in unsteady flow. *Water Resources*
719 *Research*, 27(1), 37-52. doi: 10.1029/90WR01699
- 720 Venditti, J. G., Nelson, P. A., Mearns, J. T., Wooster, J., & Dietrich, W. E. (2012).
721 Alternate bar response to sediment supply termination. *Journal of Geophysical*
722 *Research: Earth Surface*, 117(F2). doi: 10.1029/2011JF002254
- 723 Yuichi, I. (1956). Hydrodynamical study on critical tractive force. *Transactions*
724 *of the Japan Society of Civil Engineers (in Japanese)*, 1956(41), 1-21. doi:
725 10.2208/jscej1949.1956.41_1
- 726 Zhang, Z. (2000). A flexible new technique for camera calibration. *IEEE Transac-*
727 *tions on Pattern Analysis and Machine Intelligence*, 22(11), 1330-1334. doi:
728 10.1109/34.888718



Figure 1. Aerial photos in the Naka river of Japan. © Google Earth

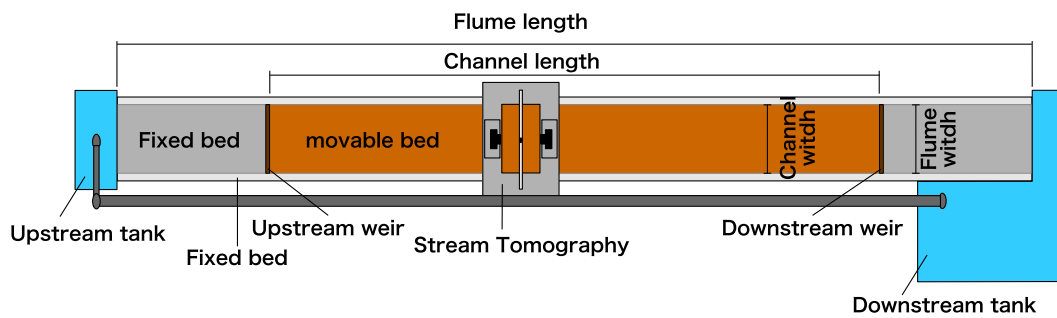


Figure 2. Plan view of the experiment flume

Appendix A Stream Tomography

Here, we describe the measurement principle of the stream tomography that was used in the flume experiment.

A1 Outline of the Measurement Device and Measurement Procedure

Figure A1 and Fig. A2 show the overall plan view of the measurement device and the layout of the equipment. The overall configuration of the measurement device consists of a laser sheet light source and a traveling platform that has two digital cameras installed. The laser sheet light source that was used in this study is a yttrium aluminum garnet (YAG) laser with a wavelength of 532 nm. In addition, in order to promote the emission of the laser light in water, the water that was used in the flume experiment was green from dissolving sodium fluorescein. As shown in Fig. A1 and Fig. A2, the two digital cameras sandwich the laser sheet light source so it

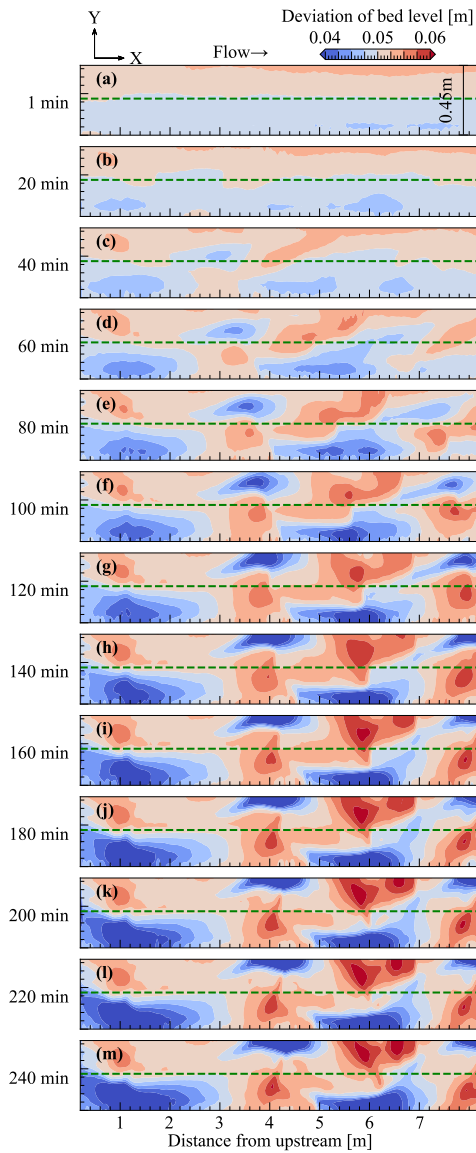


Figure 3. Temporal changes of the plan view in the observed bed topography

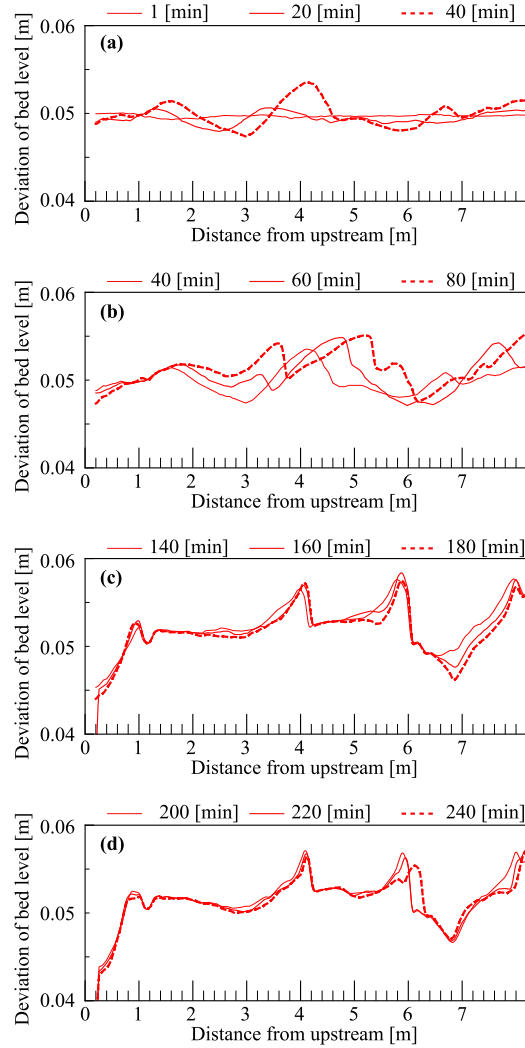


Figure 4. Longitudinal view of the measured bed shape. (a) Initial stage of the experiment, (b) occurrence of the alternate bars, (c) intermediate stage of the experiment, and (d) the final stage of the experiment

742 was upstream and downstream on the traveling platform. The camera was installed
 743 so that it looks diagonally downward toward the center of the stream. The three-
 744 dimensional coordinates of the water level and bed level by the ST can be obtained
 745 based on the intersection of the origin coordinates (lens center point) for each of the
 746 two aforementioned cameras and the geometric vector that connects the water level
 747 and bed position that will be measured.

748 ST is a non-contact measurement method that is based on triangulation and
 749 it is used for photogrammetry. The geometric relationship in this method is shown
 750 in the figures. The water level is obtained as the intersection of the two geometric
 751 vectors that connect the origin coordinates for each of the two cameras and the wa-
 752 ter surface. The bed level can be determined as the intersection of the two geometric
 753 vectors for the aforementioned water level and bed level. From these, the calculation

754 of the three-dimensional coordinates of the bed level requires consideration of the
 755 refraction of the irradiation light on the water surface. The three-dimensional coor-
 756 dinates of the bed level can be obtained using a geometric vector that considers the
 757 refraction of the irradiation light. This refraction is based on the surface water level
 758 that was obtained by this method.

759 The measurement procedures consist of the following three stages. 1) Movie
 760 shooting: a camera was installed on the traveling platform while running it in the
 761 longitudinal direction. 2) Image analysis: after decomposing the shot video into still
 762 photos, the pixel number that corresponds to the intersection of the bed and water
 763 with laser light is calculated. 3) The water level and bed level are obtained by trian-
 764 gulation. The following sections show the geometric calculations based on the image
 765 analysis and triangulation. In addition, it can be obtained either before or after the
 766 movie shooting that was described in 1). Zhang’s calibration method (Zhang, 2000)
 767 was used to calculate the internal and external parameters of the camera. The ori-
 768 gin coordinates of the cameras that were installed on the upstream and downstream
 769 sides of the waterway are \mathbf{c}_u and \mathbf{c}_d , respectively. \mathbf{c}_u and \mathbf{c}_d are the number vectors
 770 whose components are three-dimensional spatial coordinates, and $\mathbf{c}_u = (x_{c_u}, y_{c_u}, z_{c_u})$
 771 and $\mathbf{c}_d = (x_{c_d}, y_{c_d}, z_{c_d})$.

772 A2 Geometric Calculation of the Water Level and Bed Level based 773 on the Image Analysis and Triangulation

774 The method for detecting the water surface and bed surface in the ST is de-
 775 scribed as follows. From the still photograph that was created from the moving im-
 776 age captured by the camera, the pixel number corresponding to the intersection of
 777 the laser beam and the water surface, and the intersection of the laser beam and the
 778 water bed was calculated. First, the pixel number (i_w, j_w) corresponding to the in-
 779 tersection of the laser beam and the water surface is detected using the green bright-
 780 ness of the photograph as the threshold value. Similarly, the pixel numbers (i_b, j_b)
 781 corresponding to the intersection of the laser beam and the bed surface are distin-
 782 guished from the position of the maximum green brightness. The reflection inten-
 783 sity on the water surface and bed surface varies depending on the environment, laser
 784 light intensity, and the riverbed material. Therefore, it is necessary to adjust the
 785 thresholds for detecting the water and bed surfaces according to the measurement
 786 conditions. The threshold value for the green lightness in this analysis was set to
 787 40–210.

788 Next, the geometric calculation of the water level is explained. The water level
 789 was calculated from the geometric relationship that is shown in Fig. A4. The three-
 790 dimensional coordinates of the water level \mathbf{h} are obtained as the intersection of \mathbf{c}_{wu}
 791 and \mathbf{c}_{wd} . \mathbf{c}_{wu} is a geometric vector connecting \mathbf{c}_u and the water surface level to be
 792 measured \mathbf{c}_u . \mathbf{c}_{wd} is a geometric vector connecting \mathbf{c}_d and the water surface level
 793 to be measured \mathbf{c}_d . In this method, the nearest points \mathbf{h}_u and \mathbf{h}_d for these geomet-
 794 ric vectors were calculated. The threshold values are set, which can be regarded as
 795 the closest distance between the two points; the intersections are identified \mathbf{h} when
 796 it is below the threshold value. The latest points are calculated using the following
 797 equations.

$$798 \quad \mathbf{h}_u = \mathbf{c}_u + d_{cu}\hat{\mathbf{c}}_{wu} \quad (\text{A1})$$

$$799 \quad \mathbf{h}_d = \mathbf{c}_d + d_{cd}\hat{\mathbf{c}}_{wd} \quad (\text{A2})$$

$$800 \quad d_{cu} = \frac{(\hat{\mathbf{c}}_{wd} \cdot \hat{\mathbf{c}}_{wu})(\hat{\mathbf{c}}_{wd} \cdot \mathbf{c}_d\vec{\mathbf{c}}_u) - \hat{\mathbf{c}}_{wu} \cdot \mathbf{c}_d\vec{\mathbf{c}}_u}{1 - (\hat{\mathbf{c}}_{wd} \cdot \hat{\mathbf{c}}_{wu})(\hat{\mathbf{c}}_{wd} \cdot \hat{\mathbf{c}}_{wu})} \quad (\text{A3})$$

$$801 \quad d_{cd} = \frac{(\hat{\mathbf{c}}_{wu} \cdot \hat{\mathbf{c}}_{wd})(\hat{\mathbf{c}}_{wu} \cdot \mathbf{c}_u\vec{\mathbf{c}}_d) - \hat{\mathbf{c}}_{wd} \cdot \mathbf{c}_u\vec{\mathbf{c}}_d}{1 - (\hat{\mathbf{c}}_{wu} \cdot \hat{\mathbf{c}}_{wd})(\hat{\mathbf{c}}_{wu} \cdot \hat{\mathbf{c}}_{wd})} \quad (\text{A4})$$

805
 806

$$\mathbf{h} = \frac{1}{2}(\mathbf{h}_u + \mathbf{h}_d) \quad (\text{A5})$$

 807
 808
 809
 810

where \mathbf{h} is a number vector whose components are the three-dimensional coordinates of the calculated water level, and \mathbf{h}_u and \mathbf{h}_d are the number vectors of the bed level. These are calculated based on the origin coordinates of the upstream and downstream cameras. In addition, $\mathbf{c}_{\hat{w}u}$ and $\mathbf{c}_{\hat{w}d}$ are the unit vectors of \mathbf{c}_{wu} and \mathbf{c}_{wd} .

 811
 812
 813
 814
 815
 816
 817

The water level in the transverse direction is calculated using the aforementioned calculation. This calculation is repeated for the image that is taken by the traveling platform that is moving at a constant speed. As a result, transverse water surface shapes in multiple longitudinal directions were obtained, and the surface shape of the water level was obtained by combining these. During the final processing, $H_{(i,j)}$ is obtained. This is a structural discrete function that is rearranged in a grid pattern at arbitrary intervals that is based on \mathbf{h} .

 818
 819
 820
 821
 822

Next, the geometric calculation of the bed level is explained. The bed level was calculated from the geometric relationship as shown in Fig. A5. As illustrated in the figure, \mathbf{c}_{biu} and \mathbf{c}_{bid} , which are the geometric vectors that are incident in water, are refracted on the water surface. The intersections of the geometric vector after refracting from \mathbf{c}_{bru} and \mathbf{c}_{brd} are the bed pixels (i_b, j_b) on the image.

 823
 824
 825
 826
 827

Therefore, to calculate the bed level, it is necessary to obtain the geometric vectors \mathbf{c}_{bru} and \mathbf{c}_{brd} . Here, to prepare for the aforementioned calculation, the intersections \mathbf{c}_{hu} and \mathbf{c}_{hd} for the water surface and both of the geometric vectors \mathbf{c}_{biu} and \mathbf{c}_{bid} can be calculated. \mathbf{c}_{bru} and \mathbf{c}_{brd} can be calculated from the following equations while using $H_{(i,j)}$, which is arranged in a grid, and \mathbf{c}_{biu} and \mathbf{c}_{bid} .

828

$$\hat{\mathbf{c}}_{hu} = \mathbf{c}_u + \mathbf{c}_{biu} \frac{\overrightarrow{H_{(i,j)} \mathbf{c}_u \cdot \mathbf{n}_u}}{\overrightarrow{H_{(i,j)} \mathbf{c}_u \cdot \mathbf{n}_u} + \overrightarrow{H_{(i,j)} \mathbf{c}_{eu} \cdot \mathbf{n}_u}} \quad (\text{A6})$$

829

$$\mathbf{a}_{u1} = \overrightarrow{H_{(i,j)} H_{(i+1,j)}} \times \overrightarrow{H_{(i+1,j)} \hat{\mathbf{c}}_{hu}} \quad (\text{A7})$$

830

$$\mathbf{a}_{u2} = \overrightarrow{H_{(i+1,j)} H_{(i,j+1)}} \times \overrightarrow{H_{(i,j+1)} \hat{\mathbf{c}}_{hu}} \quad (\text{A8})$$

831

832

$$\mathbf{a}_{u3} = \overrightarrow{H_{(i,j+1)} H_{(i,j)}} \times \overrightarrow{H_{(i,j)} \hat{\mathbf{c}}_{hu}} \quad (\text{A9})$$

833

834

$$\mathbf{b}_{u1} = \overrightarrow{H_{(i+1,j+1)} H_{(i,j+1)}} \times \overrightarrow{H_{(i,j+1)} \hat{\mathbf{c}}_{hu}} \quad (\text{A10})$$

835

836

$$\mathbf{b}_{u2} = \overrightarrow{H_{(i,j+1)} H_{(i+1,j)}} \times \overrightarrow{H_{(i+1,j)} \hat{\mathbf{c}}_{hu}} \quad (\text{A11})$$

837

838

$$\mathbf{b}_{u3} = \overrightarrow{H_{(i+1,j)} H_{(i+1,j+1)}} \times \overrightarrow{H_{(i+1,j+1)} \hat{\mathbf{c}}_{hu}} \quad (\text{A12})$$

839

840

841

if ($\hat{\mathbf{a}}_{u1} = \hat{\mathbf{a}}_{u2} = \hat{\mathbf{a}}_{u3}$) or ($\hat{\mathbf{b}}_{u1} = \hat{\mathbf{b}}_{u2} = \hat{\mathbf{b}}_{u3}$) then,

842

$$\mathbf{c}_{hu} = \hat{\mathbf{c}}_{hu} \quad (\text{A13})$$

843

$$\hat{\mathbf{c}}_{hd} = \mathbf{c}_d + \mathbf{c}_{bid} \frac{\overrightarrow{H_{(i,j)} \mathbf{c}_d \cdot \mathbf{n}_d}}{\overrightarrow{H_{(i,j)} \mathbf{c}_d \cdot \mathbf{n}_d} + \overrightarrow{H_{(i,j)} \mathbf{c}_{ed} \cdot \mathbf{n}_d}} \quad (\text{A14})$$

844

$$\mathbf{a}_{d1} = \overrightarrow{H_{(i,j)} H_{(i+1,j)}} \times \overrightarrow{H_{(i+1,j)} \hat{\mathbf{c}}_{hd}} \quad (\text{A15})$$

845

846

$$\mathbf{a}_{d2} = \overrightarrow{H_{(i+1,j)} H_{(i,j+1)}} \times \overrightarrow{H_{(i,j+1)} \hat{\mathbf{c}}_{hd}} \quad (\text{A16})$$

847

848

$$\mathbf{a}_{d3} = \overrightarrow{H_{(i,j+1)} H_{(i,j)}} \times \overrightarrow{H_{(i,j)} \hat{\mathbf{c}}_{hd}} \quad (\text{A17})$$

849

850

$$\mathbf{b}_{d1} = \overrightarrow{H_{(i+1,j+1)} H_{(i,j+1)}} \times \overrightarrow{H_{(i,j+1)} \hat{\mathbf{c}}_{hd}} \quad (\text{A18})$$

851

852

$$\mathbf{b}_{d2} = \overrightarrow{H_{(i,j+1)} H_{(i+1,j)}} \times \overrightarrow{H_{(i+1,j)} \hat{\mathbf{c}}_{hd}} \quad (\text{A19})$$

853

854

855

$$\mathbf{b}_{d3} = \overrightarrow{H_{(i+1,j)} H_{(i+1,j+1)}} \times \overrightarrow{H_{(i+1,j+1)} \hat{\mathbf{c}}_{hd}} \quad (\text{A20})$$

856

if $(\hat{\mathbf{a}}_{d1} = \hat{\mathbf{a}}_{d2} = \hat{\mathbf{a}}_{d3})$ or $(\hat{\mathbf{b}}_{d1} = \hat{\mathbf{b}}_{d2} = \hat{\mathbf{b}}_{d3})$ then,

857

$$\mathbf{c}_{hd} = \hat{\mathbf{c}}_{hd} \quad (\text{A21})$$

858

859

$$\mathbf{c}_{hu} = \mathbf{c}_{hu} + \hat{\mathbf{c}}_{bu} \left(\frac{\overrightarrow{p_{u1} c_u} \cdot \mathbf{n}_u}{\overrightarrow{p_{u1} c_u} \cdot \mathbf{n}_u + \overrightarrow{p_{u1} c_{eu}} \cdot \mathbf{n}_u} \right) \quad (\text{A22})$$

860

861

$$\mathbf{c}_{hd} = \mathbf{c}_{hd} + \hat{\mathbf{c}}_{bd} \left(\frac{\overrightarrow{p_{d1} c_d} \cdot \mathbf{n}_d}{\overrightarrow{p_{d1} c_d} \cdot \mathbf{n}_d + \overrightarrow{p_{d1} c_{ed}} \cdot \mathbf{n}_d} \right) \quad (\text{A23})$$

862

863

864

865

where \mathbf{c}_{hu} , $\hat{\mathbf{c}}_{hu}$, \mathbf{c}_{hd} , and $\hat{\mathbf{c}}_{hd}$ represent a number vector with three-dimensional coordinates. These are the starting points of the geometric vectors \mathbf{c}_{bru} and \mathbf{c}_{brd} , and p_1 , p_2 , and p_3 are the three-dimensional coordinates of the structured water surface that defines the function of each water surface.

866

867

In the second step, using Snell's law, we can calculate \mathbf{c}_{bru} and \mathbf{c}_{brd} with the following equations.

868

$$\mathbf{c}_{bru} = \frac{1}{n_0} \{ \mathbf{c}_{biu} + (e_u - m_u) \mathbf{n}_u \} \quad (\text{A24})$$

869

870

871

$$e_u = -(\mathbf{c}_{biu} \cdot \mathbf{n}_u) \quad (\text{A25})$$

872

873

$$m_u = \sqrt{n_0^2 + e_u^2} - 1 \quad (\text{A26})$$

874

875

876

877

$$\mathbf{c}_{brd} = \frac{1}{n_0} \{ \mathbf{c}_{bid} + (e_d - m_d) \mathbf{n}_d \} \quad (\text{A27})$$

$$e_d = -(\mathbf{c}_{bid} \cdot \mathbf{n}_d) \quad (\text{A28})$$

878

879

880

$$m_d = \sqrt{n_0^2 + e_d^2} - 1 \quad (\text{A29})$$

$$n_0 = \frac{n_2}{n_1} \quad (\text{A30})$$

881

882

n_1 and n_2 are $n_1 = 1.0$ and $n_2 = 1.33$, which represent the refractive indices of air and water, respectively.

883

884

Furthermore, in the third step, \mathbf{b}_u and \mathbf{b}_d , which is the closest distance between \mathbf{c}_{bru} and \mathbf{c}_{brd} , is calculated using the following equation.

885

$$\mathbf{b}_u = \mathbf{c}_{hu} + \mathbf{d}_{u2} \hat{\mathbf{c}}_{bru} \quad (\text{A31})$$

886

887

888

$$\mathbf{b}_d = \mathbf{c}_{hd} + \mathbf{d}_{d2} \hat{\mathbf{c}}_{brd} \quad (\text{A32})$$

889

890

$$\mathbf{d}_{u2} = \frac{(\hat{\mathbf{c}}_{bru} \cdot \hat{\mathbf{c}}_{brd})(\hat{\mathbf{c}}_{brd} \cdot \mathbf{c}_{hd} \vec{\mathbf{c}}_{hu}) - \hat{\mathbf{c}}_{bru} \cdot \mathbf{c}_{hd} \vec{\mathbf{c}}_{hu}}{1 - (\hat{\mathbf{c}}_{bru} \cdot \hat{\mathbf{c}}_{brd})(\hat{\mathbf{c}}_{bru} \cdot \hat{\mathbf{c}}_{brd})} \quad (\text{A33})$$

891

892

$$\mathbf{d}_{d2} = \frac{(\hat{\mathbf{c}}_{bru} \cdot \hat{\mathbf{c}}_{brd})(\hat{\mathbf{c}}_{bru} \cdot \mathbf{c}_{hu} \vec{\mathbf{c}}_{hd}) - \hat{\mathbf{c}}_{brd} \cdot \mathbf{c}_{hu} \vec{\mathbf{c}}_{hd}}{1 - (\hat{\mathbf{c}}_{bru} \cdot \hat{\mathbf{c}}_{brd})(\hat{\mathbf{c}}_{bru} \cdot \hat{\mathbf{c}}_{brd})} \quad (\text{A34})$$

893

$$\mathbf{b} = \frac{1}{2} (\mathbf{b}_u + \mathbf{b}_d) \quad (\text{A35})$$

894

895

896

where \mathbf{b}_u , \mathbf{b}_d , and \mathbf{b} are the number vectors whose components are the three-dimensional coordinates of the bed level, $\hat{\mathbf{b}}_{bru}$, and $\hat{\mathbf{b}}_{brd}$ represents the unit vectors \mathbf{b}_{bru} and \mathbf{b}_{brd} .

897

898

899

900

In this method, the nearest points \mathbf{b}_u and \mathbf{b}_d for both the vectors were calculated. If the distance between the two points below the threshold values, which can be regarded as the distance between the two points, is set sufficiently, \mathbf{b} is identified as an intersection for both the points.

901

902

From the aforementioned, the ST acquired the three-dimensional coordinates of the water surface and bed surface.

903 **A3 Verification of the Measurement Accuracy**

904 ***A31 Experiment Outline***

905 The measurement accuracy of the water level and bed level of the ST for the
 906 alternate bars was verified using the following procedure. The channel that was used
 907 in the experiment was the same that was used in this study. In the movable bed ex-
 908 periment, in which the alternate bars were formed prior to the verification of the
 909 measurement accuracy, the channel slope was set to 1/200, the flow discharge was
 910 set to 1.7 L/s, and the riverbed material with an average particle size of 0.76 mm
 911 was used.

912 The bed shape that was measured consisted of a fixed bed was created by sprin-
 913 kling thinly the cement powder. This bed shape is the alternate bars after 120 min
 914 when the water flow started from a flat floor. Immobilization with cement powder
 915 was carried out in a section that was 2 m in the central part of the waterway used in
 916 this experiment.

917 After confirming the adhesion of the cement powder, the water flow was restarted,
 918 and the water level and bed level were measured using the ST and point gauge. The
 919 measurement with the point gauge was set at intervals of 10 cm in the longitudinal
 920 direction and 2 cm in the transverse direction to capture the geometrical features of
 921 the alternate bars. The measurement section in the longitudinal direction was 200
 922 cm for one wavelength of the alternate bar, which formed in the experimental chan-
 923 nel. In addition, the measurement section in the transverse direction was 40 cm at
 924 the center of the channel. This was not affected by the reflection of the irradiation
 925 laser from the upper surface of the channel by the side wall. The ST measurement
 926 interval was set to 1 cm in the longitudinal and transverse directions.

927 ***A32 Measurement Results***

928 Figure A6 shows the measurement results of the water surface and bed surface.
 929 In the figure, (a) and (b) are the shapes of the photographed water surface in the
 930 flow and the bed surface after drainage, and (c) and (d) display the water surface
 931 and bed surface levels that was measured by ST. In addition, (e) and (f) present the
 932 water surface and bed surface levels that were measured by the point gauge. Finally,
 933 (g) and (h) display the difference between the point gauge and ST for the water sur-
 934 face and bed surface levels.

935 As shown in Fig. A6, a wave sequence of the standing waves with a wavelength
 936 of approximately 7–10 cm is formed on the water surface in the water flow in the
 937 longitudinal direction. In addition, from (b), it can be observed that the alternate
 938 bars with a sedimentary height of approximately 0.5 cm are formed on the left bank
 939 side. It should be noted that the characteristic shape of the front edge and small
 940 undulations formed on the bars.

941 Next, by comparing (c), (d), (e), and (f) in the figure, the undulations of the
 942 high waves that are several centimeters in height cannot be reproduced at the wa-
 943 ter level and bed level at the measurement point intervals of the point gauge. Con-
 944 versely, it can be reproduced in ST. For the measurement targets in this study, the
 945 wave with the shortest wavelength is the standing wave on the water surface. It can
 946 be observed that this wave can be reproduced well with a resolution of 1 cm, which
 947 can provide 10 measurement points in this wave. Figures A7 (a) and (b) show the
 948 histograms that were created from Fig. A6 (g) and (h), respectively. In this exper-
 949 iment, the water surface was constantly changing; it did not have a constant shape.
 950 Because a vertical fluctuation of approximately 2 mm was observed at the maximum
 951 point, the point gauge was measured to capture the center of the fluctuation range.

952 For this reason, Fig. A7 (a) shows the effect of the time fluctuations on the water
 953 surface. Therefore, even if there is no measurement error, it should be noted that
 954 the difference between the point gauge and the ST measurement value does not be-
 955 come 0.

956 By looking at the difference between ST and the point gauge, μ is -0.005 cm, σ
 957 is 0.063 cm for the water level measurement, μ is -0.203 cm, and σ is 0.093 cm when
 958 the bed level measurement is performed. When the measured value of the point
 959 gauge is used as the standard of the ST measurement accuracy, the measurement
 960 accuracy of the bed level is lower than the water level from the aforementioned re-
 961 sults. However, it can be observed that the measurement accuracy is approximately
 962 10 % of the maximum wave height of the alternate bars. From this, it can be con-
 963 cluded that this method has a sufficient measurement accuracy to measure alternate
 964 bars.

965 **Appendix B Validity of the Pseudo-steady Flow Assumption that** 966 **is applied to the Bars-Scale Riverbed Waves**

967 This section describes the validity of the pseudo-steady flow assumption that
 968 is applied to the bars-scale riverbed waves. In this study, we introduced the assump-
 969 tion of a pseudo-steady flow when deriving the HPDE for the bed level z . This as-
 970 sumption is often introduced in stability analyses of bars-scale riverbed waves (Callander,
 971 1969; Kuroki & Kishi, 1984). In the aforementioned stability analysis, it is assumed
 972 that the migration speed of the bed is sufficiently slower than the propagation ve-
 973 locity of the flow, and the flow can be treated as a pseudo-steady flow if the flow
 974 rate is constant. Based on this assumption, the stability analysis ignores the term
 975 of the time gradient in the continuity equation of flow and the equation of motion
 976 of flow among the governing equations that are used in the analysis. The aforemen-
 977 tioned assumptions are considered to be valid. This is because the stability analysis
 978 explains the occurrence and developmental mechanisms of the alternate bars. How-
 979 ever, to the best of our knowledge, whether the term of the time gradient of the flow
 980 can actually be ignored cannot be confirmed from the actual phenomenon. There-
 981 fore, we verified whether the term of the flow time gradient can be ignored with the
 982 ST measurement values and hydraulic analysis.

983 The aforementioned verification was performed by comparing the contributions
 984 of each term in the equation of motion for the flow.

$$985 \quad \frac{1}{g} \frac{\partial u}{\partial t} + \frac{u}{g} \frac{\partial u}{\partial x} + \frac{\partial H}{\partial x} + I_{ex} = 0 \quad (\text{B1})$$

986 H is the water level. As an explanation of the various physical quantities has al-
 987 ready been mentioned, it is omitted here. The contribution of each term in the afore-
 988 mentioned equation was calculated for each ST measurement time, and the magni-
 989 tudes were compared.

990 $\partial H/\partial x$ was obtained with the measured value of the water level of the ST.
 991 Other terms was obtained with the results of the hydraulic analysis, which is de-
 992 scribed in Section 4.1 in the main text. The time interval and spatial interval of the
 993 calculation were 1 min and 2 cm, which are the time resolutions and spatial reso-
 994 lutions of ST. The flow velocity and migration speed of the y component under the
 995 experimental conditions are 10^{-4} to 10^1 of the x components at any location regard-
 996 less of the developmental state of the alternate bars. For simplicity, the y component
 997 is ignored in this section.

998 Figure B1 shows the time change of the box-beard diagram that displays the
 999 contribution of each term. This figure shows the (a) local term, (b) advection term,
 1000 (c) pressure term, and (d) friction term; they correspond to the order of each term

1001 in Eq. (B1). By looking at the figure, although the (b) advection term, (c) pressure
 1002 term, and (d) friction term dominate the flow at any time, it can be confirmed that
 1003 (a) the local term can be ignored because the local term is smaller than the afore-
 1004 mentioned three terms. Even if the advection term with the smallest contribution in
 1005 (b),(c), and(d) is compared with the local term, the contribution of the local term is
 1006 10^{-4} to 10^{-2} of the (b) advection term. In addition, it can be observed that the lo-
 1007 cal term is extremely small. From this, it is inferred that it is physically appropriate
 1008 to ignore the time gradient of the flow in the alternate bars.

1009 **Appendix C Derivation of the Two-Dimensional Equation of the** 1010 **Water Surface Profile**

1011 Appendix C presents the derivation processes of the two-dimensional equa-
 1012 tion of the water surface profile to derive the HPDE for the bed level. The govern-
 1013 ing equations that were used for the derivation consist of the following continuous
 1014 equations and the equations of motion. When deriving the equation, the flow can be
 1015 treated as a pseudo-steady-state flow based on the verification results in Appendix
 1016 B. Therefore, the following continuous equations and equations of motion are used
 1017 for the derivation.

$$1018 \quad \frac{\partial[hu]}{\partial x} + \frac{\partial[hv]}{\partial y} = 0 \quad (C1)$$

$$1019 \quad \frac{u}{g} \frac{\partial u}{\partial x} + \frac{v}{g} \frac{\partial u}{\partial y} + \frac{\partial z}{\partial x} + \frac{\partial h}{\partial x} + I_{ex} = 0 \quad (C2)$$

$$1020 \quad \frac{u}{g} \frac{\partial v}{\partial x} + \frac{v}{g} \frac{\partial v}{\partial y} + \frac{\partial z}{\partial y} + \frac{\partial h}{\partial y} + I_{ey} = 0 \quad (C3)$$

1023 As an explanation of the various physical quantities has already been mentioned, it
 1024 is omitted here.

1025 The derivation of $\partial h/\partial x$ is described as follows. First, applying the product
 1026 rule to Eq. (C1) results in the following equation.

$$1027 \quad h \frac{\partial u}{\partial x} + u \frac{\partial h}{\partial x} + h \frac{\partial v}{\partial y} + v \frac{\partial h}{\partial y} = 0 \quad (C4)$$

1028 Next, for the first and third terms on the left side of Eq. (C4),

$$1029 \quad u = \frac{1}{n} I_{ex}^{1/2} h^{2/3} \quad (C5)$$

$$1030 \quad v = \frac{1}{n} I_{ey}^{1/2} h^{2/3} \quad (C6)$$

$$1031 \quad \frac{\partial u}{\partial x} = \frac{\partial u}{\partial h} \frac{\partial h}{\partial x} + \frac{\partial u}{\partial I_{ex}} \frac{\partial I_{ex}}{\partial x} = \frac{2}{3} \frac{u}{h} \frac{\partial h}{\partial x} + \frac{1}{2} \frac{u}{I_{ex}} \frac{\partial I_{ex}}{\partial x} \quad (C7)$$

$$1032 \quad \frac{\partial v}{\partial y} = \frac{\partial v}{\partial h} \frac{\partial h}{\partial y} + \frac{\partial v}{\partial I_{ey}} \frac{\partial I_{ey}}{\partial y} = \frac{2}{3} \frac{v}{h} \frac{\partial h}{\partial y} + \frac{1}{2} \frac{v}{I_{ey}} \frac{\partial I_{ey}}{\partial y} \quad (C8)$$

1036 After the differentiation of the composite function (Eq. (C7) and Eq. (C8)) using
 1037 Manning's flow velocity formula (Eq. (C5), Eq. (C6)), substituting it into Eq. (C4),
 1038 and rearranging $\partial h/\partial x$, the following equation is obtained.

$$1039 \quad \frac{\partial h}{\partial x} = -\frac{v}{u} \frac{\partial h}{\partial y} - \frac{3}{10} \frac{h}{I_{ex}} \frac{\partial I_{ex}}{\partial x} - \frac{3}{10} \frac{vh}{uI_{ey}} \frac{\partial I_{ey}}{\partial y} \quad (C9)$$

1040 Next, after substituting Eq. (C7) and the following Eq. (C10) into the first
 1041 and second terms of the equation of motion in the x direction for Eq. (C2),

$$1042 \quad \frac{\partial u}{\partial y} = \frac{\partial u}{\partial h} \frac{\partial h}{\partial y} + \frac{\partial u}{\partial I_{ex}} \frac{\partial I_{ex}}{\partial y} = \frac{2}{3} \frac{u}{h} \frac{\partial h}{\partial y} + \frac{1}{2} \frac{u}{I_{ex}} \frac{\partial I_{ex}}{\partial y} \quad (C10)$$

1043 the following equation is obtained. After substituting Eq. (C9), which was organized
 1044 earlier into Eq. (C11),

$$\begin{aligned}
 & \frac{3}{10} \frac{u^2}{gI_{ex}} \frac{\partial I_{ex}}{\partial x} - \frac{1}{5} \frac{uv}{gI_{ey}} \frac{\partial I_{ey}}{\partial y} + \frac{1}{2} \frac{uv}{gI_{ex}} \frac{\partial I_{ex}}{\partial y} + \frac{\partial z}{\partial x} \\
 & - \frac{v}{u} \frac{\partial h}{\partial y} - \frac{3}{10} \frac{h}{I_{ex}} \frac{\partial I_{ex}}{\partial x} - \frac{3}{10} \frac{vh}{uI_{ey}} \frac{\partial I_{ey}}{\partial y} + I_{ex} = 0
 \end{aligned} \tag{C11}$$

1046 The following equation can be obtained by rearranging $\partial h/\partial y$.

$$\begin{aligned}
 \frac{\partial h}{\partial y} = & \frac{3}{10} \frac{u^3}{vgI_{ex}} \frac{\partial I_{ex}}{\partial x} - \frac{1}{5} \frac{u^2}{gI_{ey}} \frac{\partial I_{ey}}{\partial y} + \frac{1}{2} \frac{u^2}{gI_{ex}} \frac{\partial I_{ex}}{\partial y} \\
 & + \frac{u}{v} \frac{\partial z}{\partial x} - \frac{3}{10} \frac{uh}{vI_{ex}} \frac{\partial I_{ex}}{\partial x} - \frac{3}{10} \frac{h}{I_{ey}} \frac{\partial I_{ey}}{\partial y} + \frac{u}{v} I_{ex}
 \end{aligned} \tag{C12}$$

1048 After substituting Eq. (C12) into Eq. (C9) and rearranging it, the following $\partial h/\partial x$
 1049 is derived.

$$\begin{aligned}
 \frac{\partial h}{\partial x} = & -\frac{\partial z}{\partial x} - I_{ex} - \frac{3}{10} \frac{u^2}{gI_{ex}} \frac{\partial I_{ex}}{\partial x} \\
 & + \frac{1}{5} \frac{uv}{gI_{ey}} \frac{\partial I_{ey}}{\partial y} - \frac{1}{2} \frac{uv}{gI_{ex}} \frac{\partial I_{ex}}{\partial y}
 \end{aligned} \tag{C13}$$

1051 By rearranging $\partial h/\partial y$ using the same process as earlier, the following equation
 1052 for $\partial h/\partial y$ is obtained.

$$\begin{aligned}
 \frac{\partial h}{\partial y} = & -\frac{\partial z}{\partial y} - I_{ey} - \frac{3}{10} \frac{v^2}{gI_{ey}} \frac{\partial I_{ey}}{\partial y} \\
 & - \frac{1}{2} \frac{uv}{gI_{ey}} \frac{\partial I_{ey}}{\partial x} + \frac{1}{5} \frac{uv}{gI_{ex}} \frac{\partial I_{ex}}{\partial x}
 \end{aligned} \tag{C14}$$

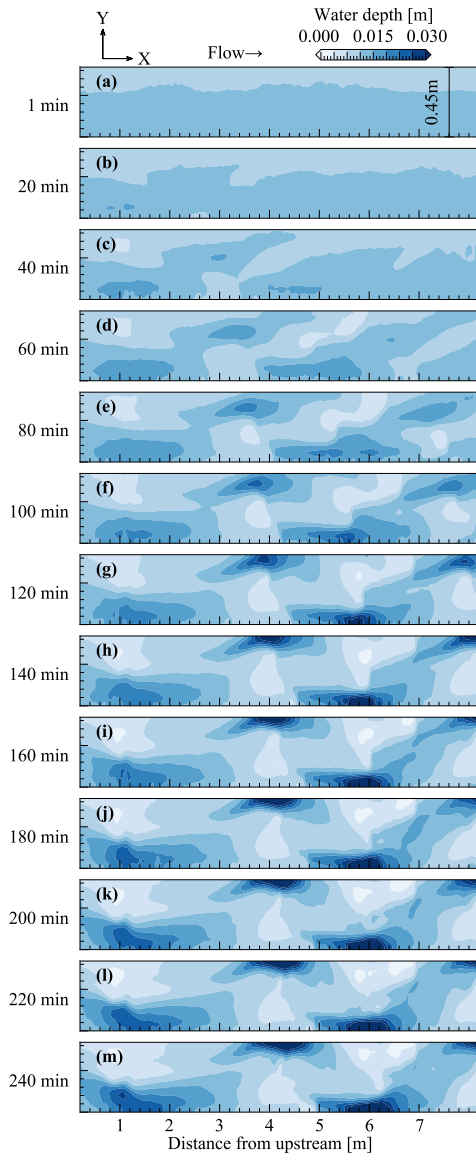


Figure 5. Temporal changes of the plan view for the observed water depth

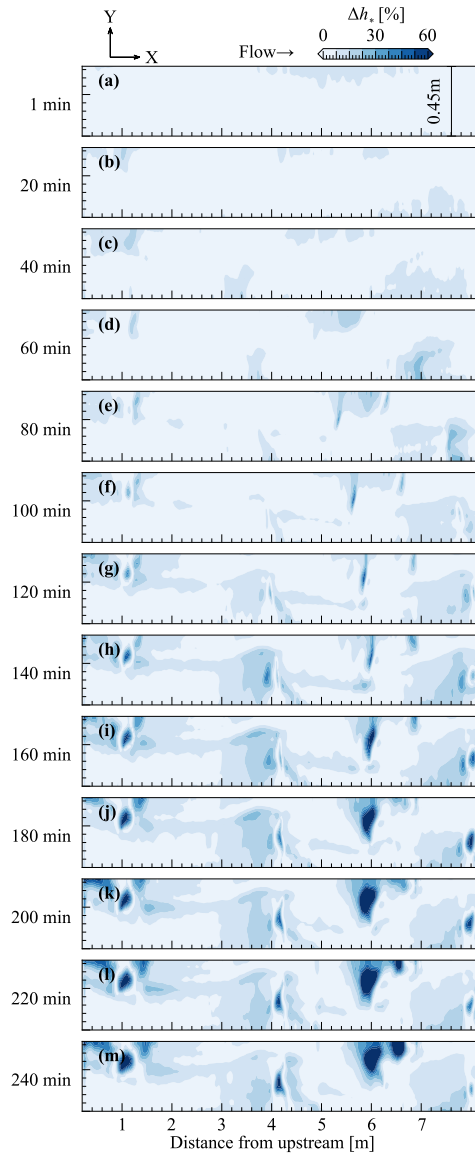


Figure 6. Difference between the measured value and the calculated value of the water depth that is made dimensionless by the measured value.

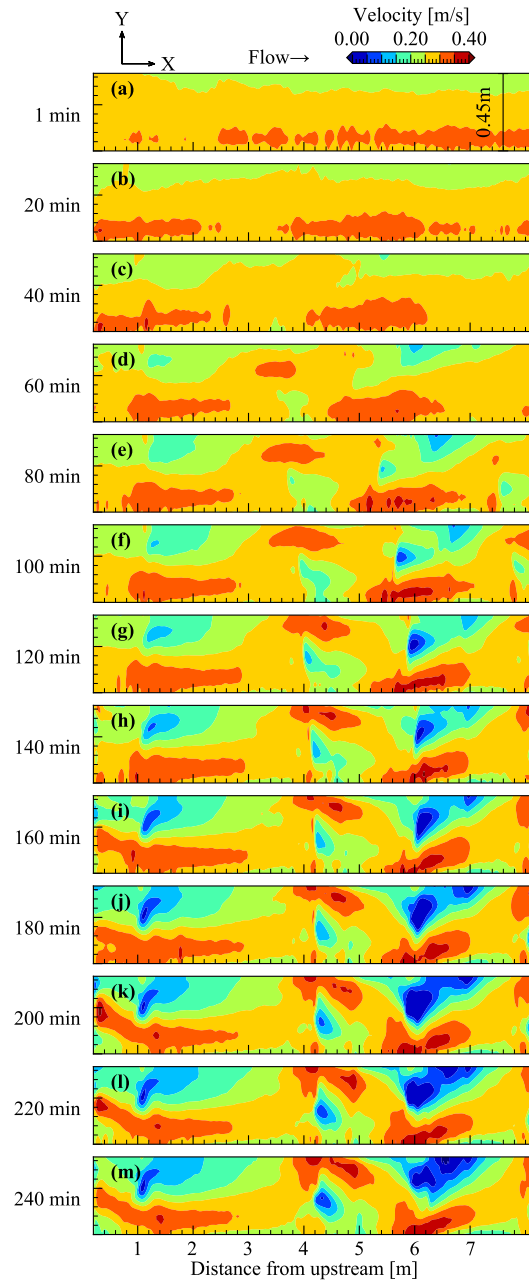


Figure 7. Temporal changes of the plan view for the calculated flow velocity

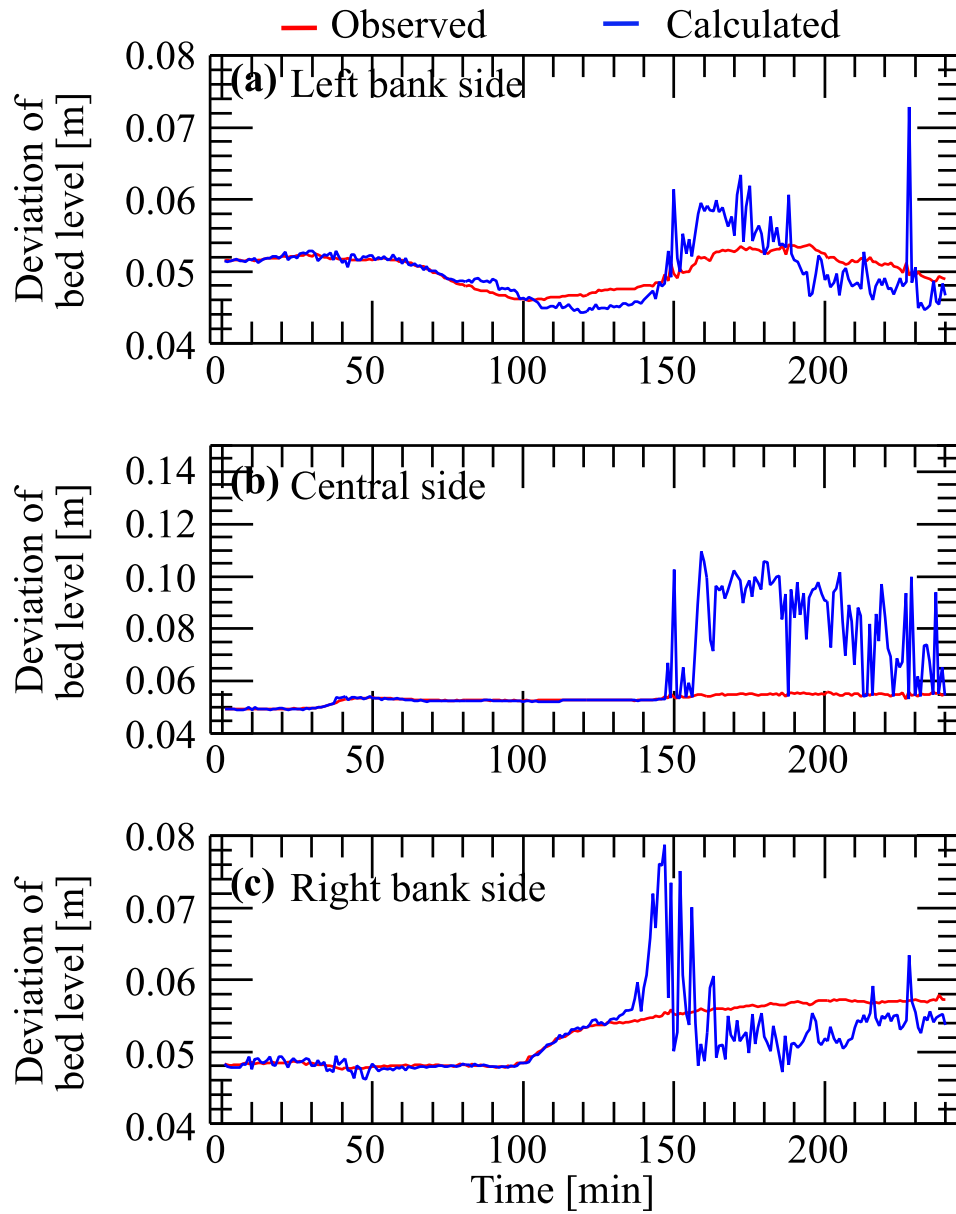


Figure 8. Bed-level time waveform. (a) Left bank side, (b) center, (c) right bank side

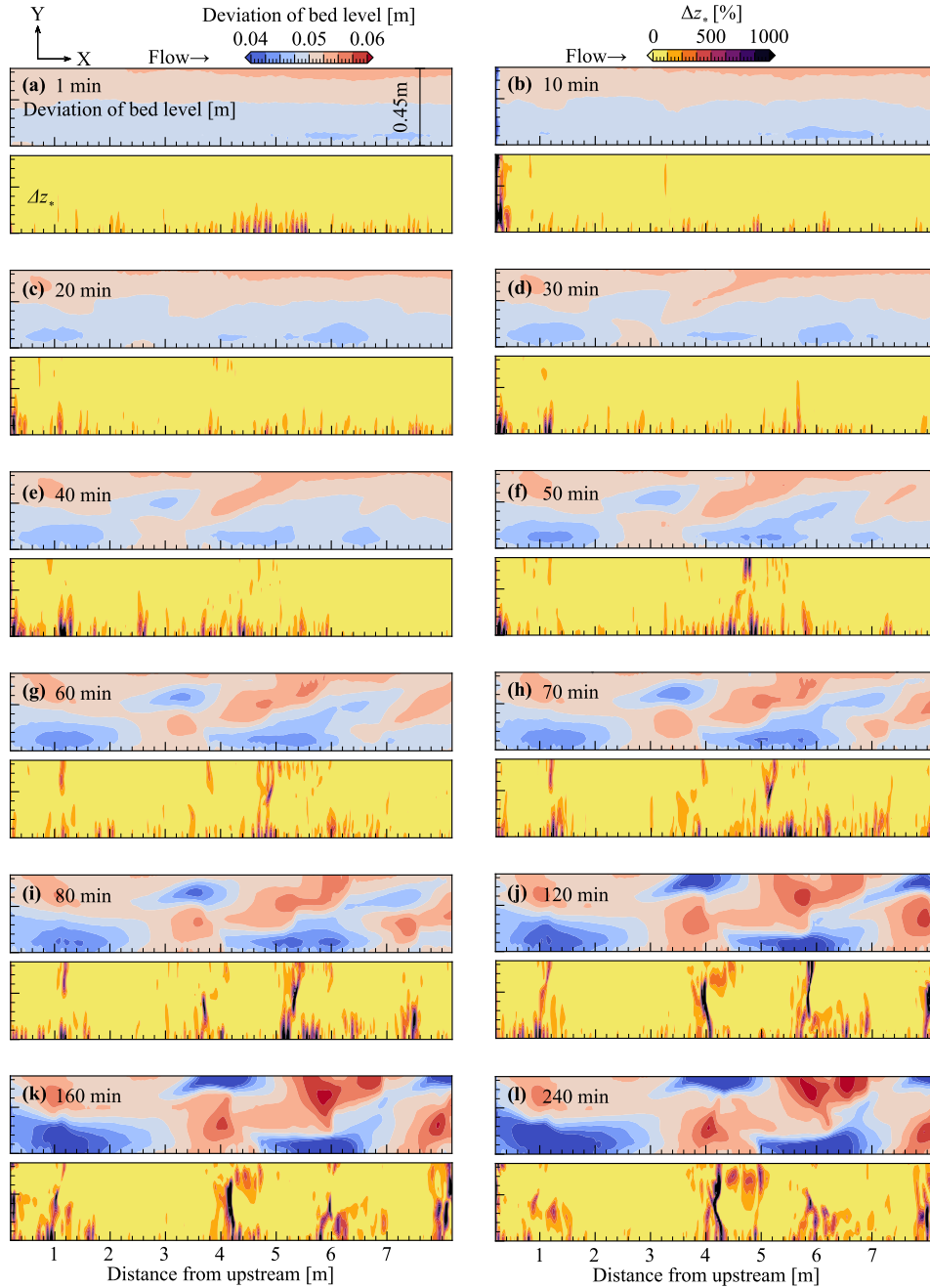


Figure 9. Temporal changes of the plan view for the observed bed topography and Δz_*

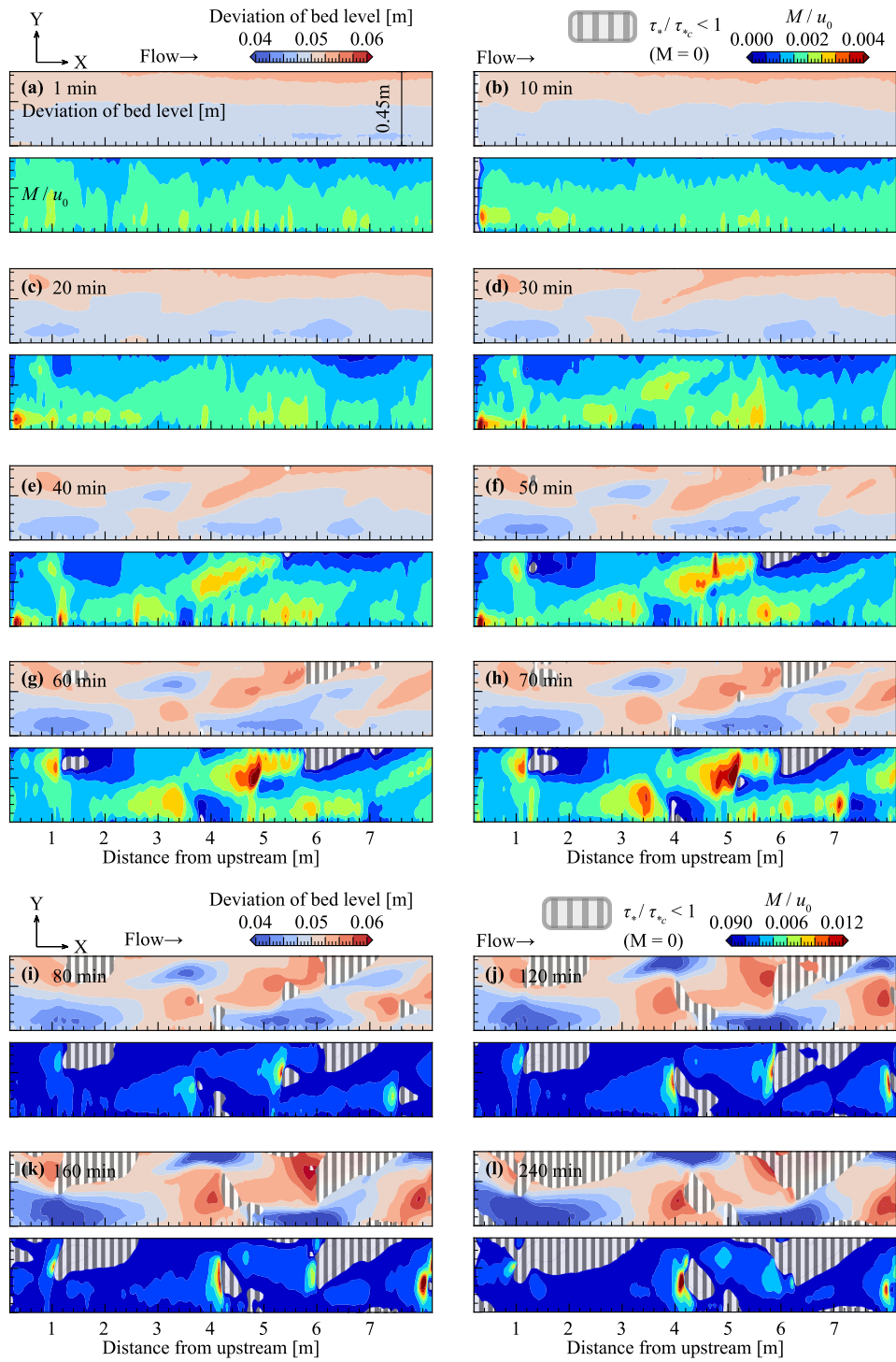


Figure 10. Temporal changes of the plan view for the observed bed topography and the calculated migrating speed

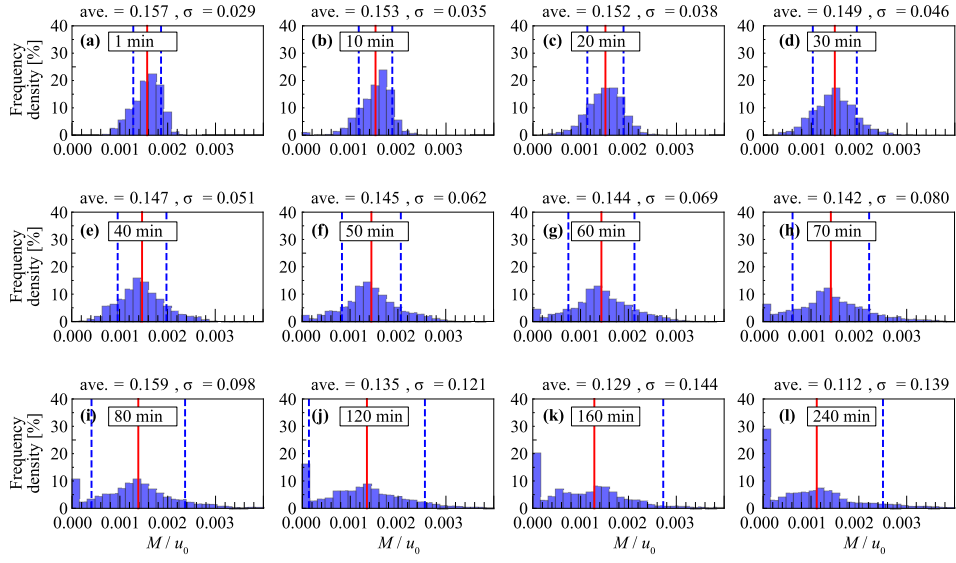


Figure 11. Histograms of the migrating speed

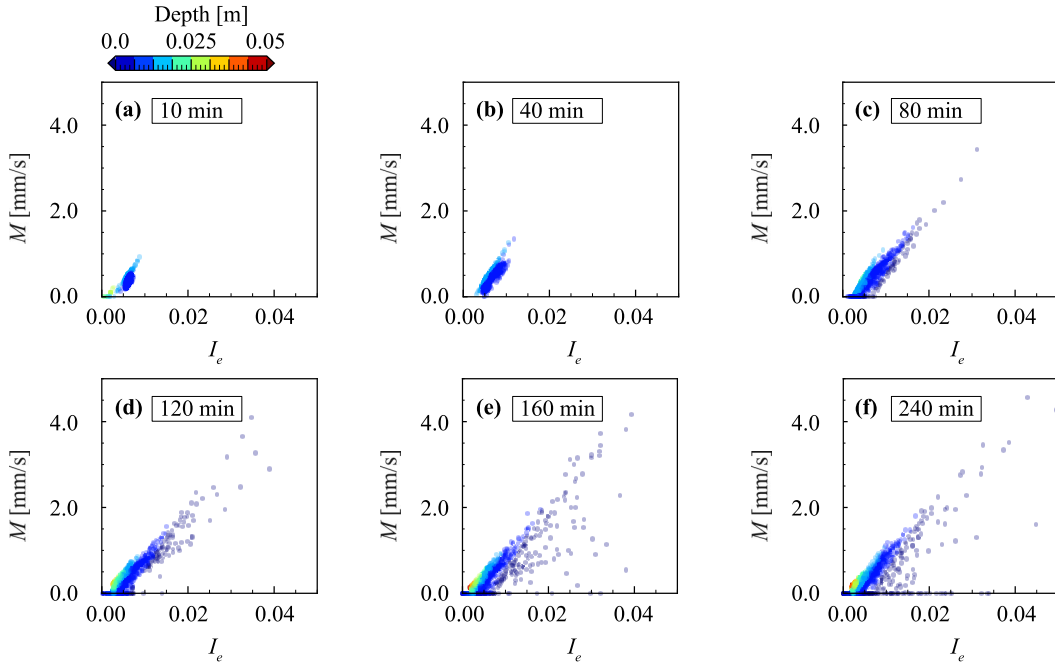


Figure 12. Relationship between the migrating speed, energy slope, and water depth

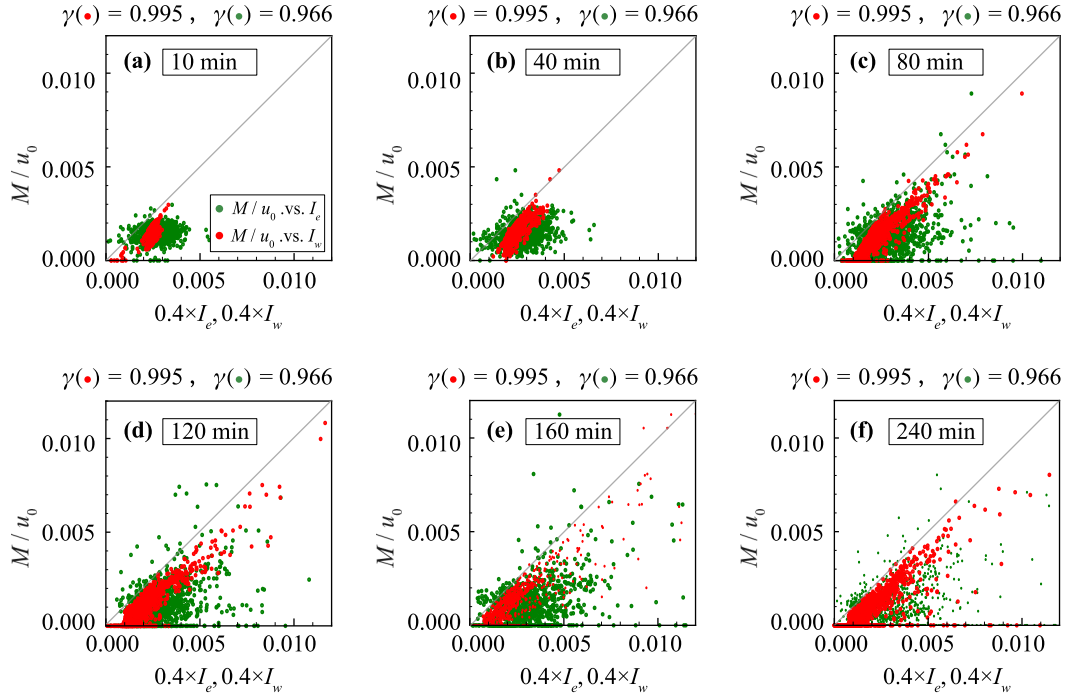


Figure 13. Relationship between the migrating speed, energy slope, and water surface slope

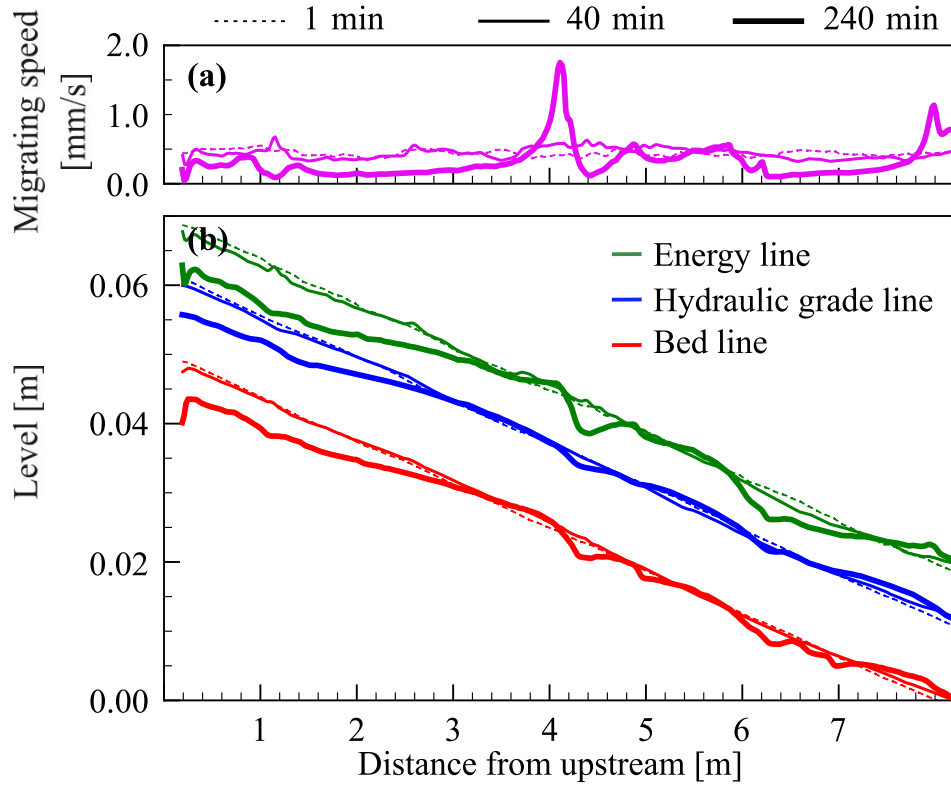


Figure 14. Longitudinal view of the (a) cross-sectional averaged migrating speed, (b) and cross-sectional averaged bed level

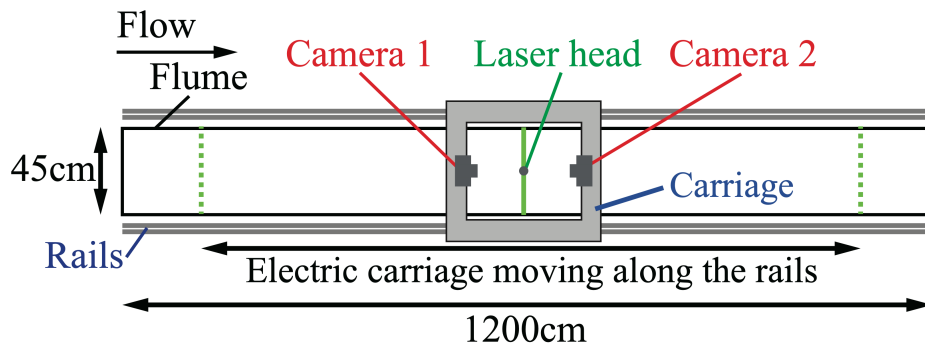


Figure A1. Overall plan view of the measurement device

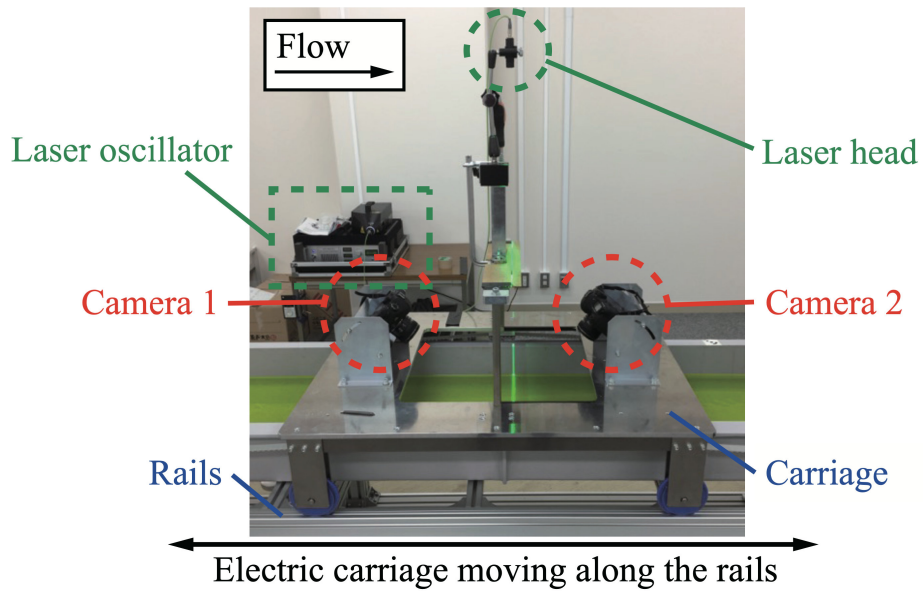


Figure A2. Equipment layout of the measurement equipment

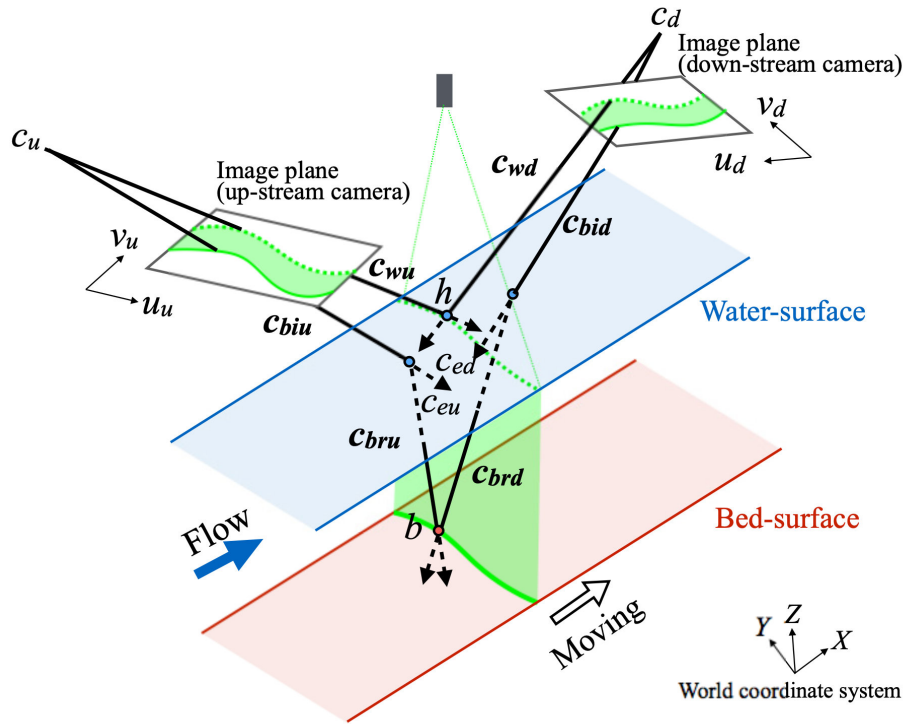


Figure A3. Outline of the measurement principle of the water surface and bed surface by triangulation

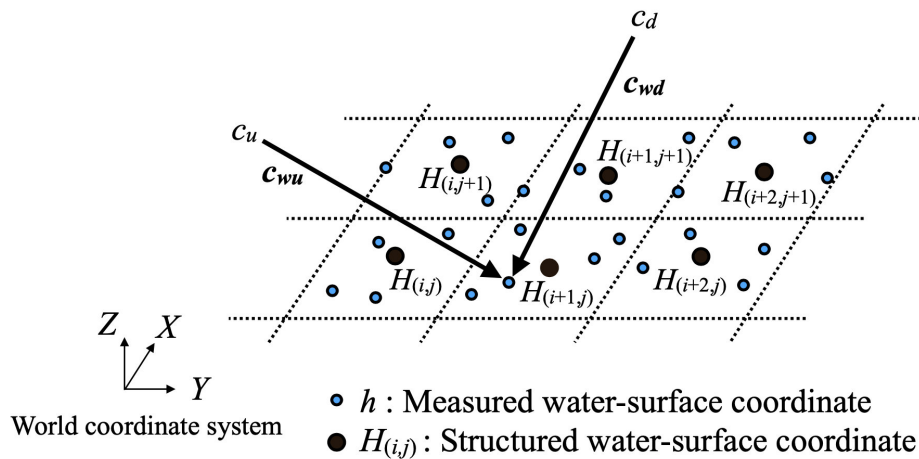


Figure A4. Relationship between h and H that is rearranged in a grid by triangulation

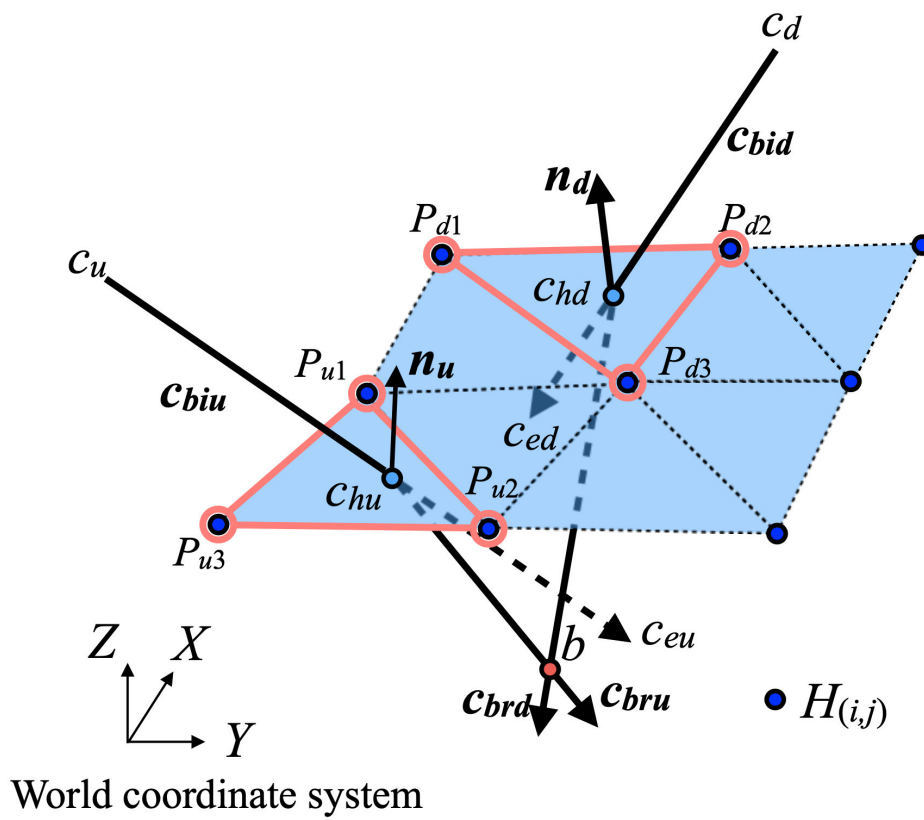


Figure A5. Outline of the bed surface measurement method while considering the refraction on the water surface

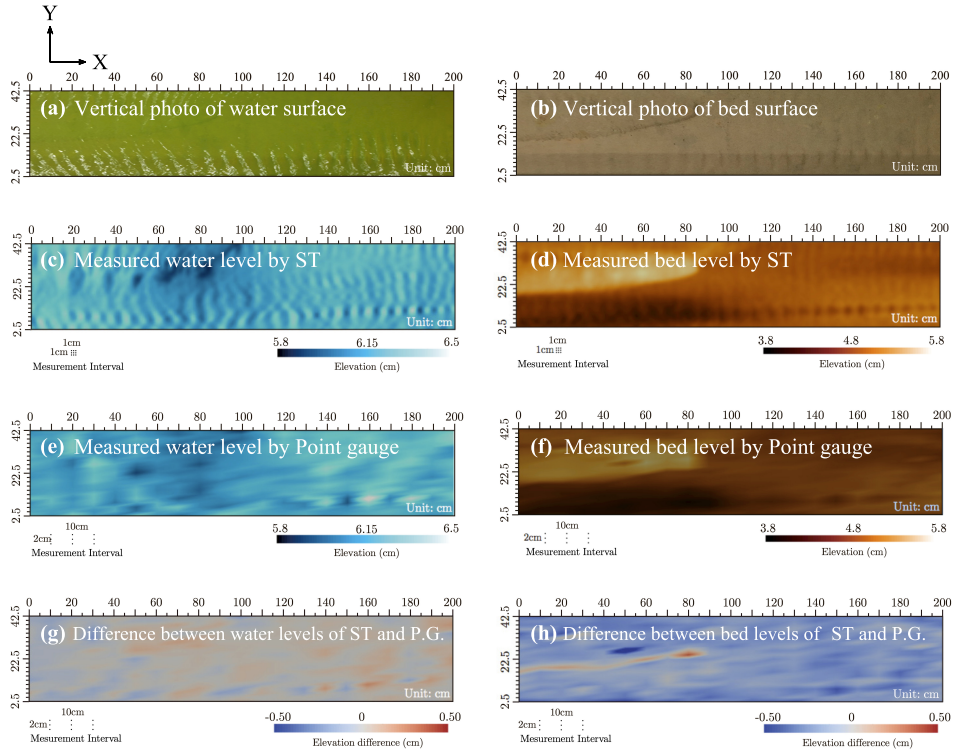


Figure A6. Measurement results of the water surface and bed surface

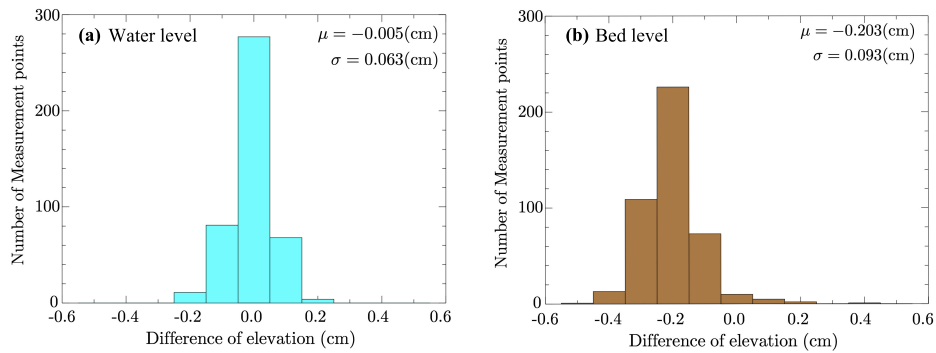


Figure A7. Histogram of the difference for the ST and point gauge measurements

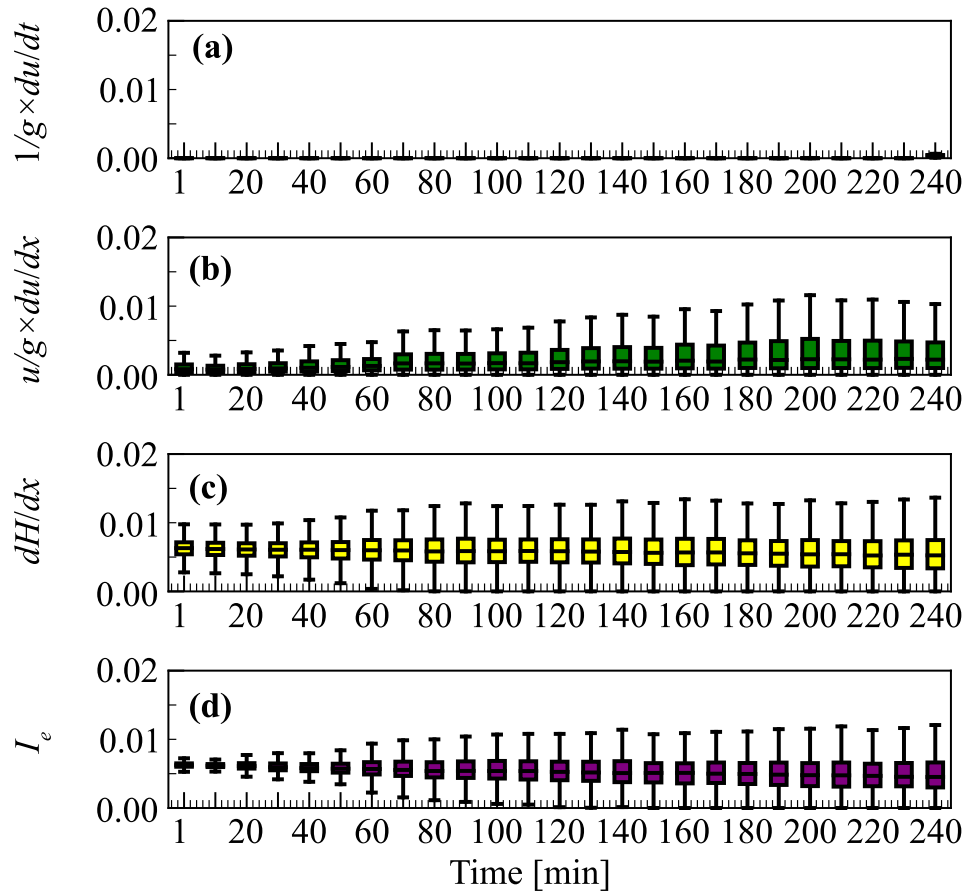


Figure B1. Temporal changes of the box plots for the (a) local term, (b) advection term, (c) pressure term, (d) and friction term